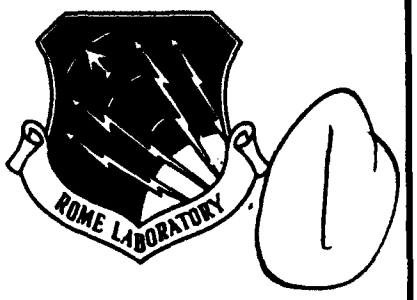

RL-TR-94-122
Final Technical Report
August 1994

CVD SILICON CARBIDE CHARACTERIZATION

University of Dayton Research Institute

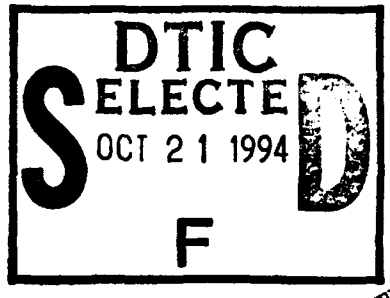

Sponsored by
Ballistic Missile Defense Organization

APPROVED FOR PUBLIC RELEASE; DISTRIBUTION UNLIMITED.

Rome Laboratory
Air Force Materiel Command
Griffiss Air Force Base, New York

. This report has been reviewed by the Rome Laboratory Public Affairs Office (PA) and is releasable to the National Technical Information Service (NTIS). At NTIS it will be releasable to the general public, including foreign nations.

RL-TR-94-122 has been reviewed and is approved for publication.

APPROVED: Richard Fedors

RICHARD FEDORS
Project Engineer

FOR THE COMMANDER: Luke L. Lucas

LUKE L. LUCAS, Colonel, USAF
Deputy Director
Surveillance & Photonics

If your address has changed or if you wish to be removed from the Rome Laboratory mailing list, or if the addressee is no longer employed by your organization, please notify RL (OCPC) Griffiss AFB NY 13441. This will assist us in maintaining a current mailing list.

Do not return copies of this report unless contractual obligations or notices on a specific document require that it be returned.

CVD SILICON CARBIDE CHARACTERIZATION

G. A. Graves
D. Iden

Contractor: University of Dayton Research Institute
Contract Number: F30602-90-D-0105, Task 6
Effective Date of Contract: 25 August 1992
Contract Expiration Date: 24 August 1993
Short Title of Work: CVD Silicon Carbide Characterization
Period of Work Covered: Aug 92 - Oct 93

Principal Investigator: G. A. Graves, Jr.
Phone: (513) 229-4415

RL Project Engineer: Donald Luczak
Phone: (315) 330-3144

This research was supported by the Ballistic Missile Defense Organization of the Department of Defense and was monitored by Richard Fedors, RL (OCPC), 25 Electronic Pky, Griffiss AFB NY 13441-4515 under Contract F30602-90-D-0105.

REPORT DOCUMENTATION PAGE

Form Approved
OMB No. 0704-0188

1. AGENCY USE ONLY (Leave Blank)	2. REPORT DATE	3. REPORT TYPE AND DATES COVERED
	August 1994	Final Aug 92 - Oct 93

4. TITLE AND SUBTITLE
CVD SILICON CARBIDE CHARACTERIZATION

5. FUNDING NUMBERS
C - F30602-90-D-0105, Task 6
PE - 63215C
PR - 1101
TA - QN
WU - 15

6. AUTHOR(S)
G. A. Graves, Jr. and D. Iden

7. PERFORMING ORGANIZATION NAME(S) AND ADDRESS(ES)
University of Dayton Research Institute
Dayton OH 45469-0172

8. PERFORMING ORGANIZATION REPORT NUMBER
UDR-TR-93-103

9. SPONSORING/MONITORING AGENCY NAME(S) AND ADDRESS(ES)
Ballistic Missile Defense Organization
7100 Defense Pentagon
Wash DC 20301-7100

Rome Laboratory (OCPC)
25 Electronic Pky
Griffiss AFB NY 13441-4515

10. SPONSORING/MONITORING AGENCY REPORT NUMBER
RL-TR-94-122

11. SUPPLEMENTARY NOTES
Prepared for Science Applications International Corporation, Rome NY 13440
Rome Laboratory Project Engineer: Richard Fedors/OCPC/(315) 330-3144

12a. DISTRIBUTION/AVAILABILITY STATEMENT
Approved for public release; distribution unlimited.

12b. DISTRIBUTION CODE

13. ABSTRACT (Maximum 200 words)

Chemically vapor deposited (CVD) silicon carbide is a candidate material for high quality ground and space-based mirror substrates and high quality reflective optics. Statistically valid material property data has not been available, however, to make durability and lifetime predictions for such optics. The primary purpose of this study was to determine the Weibull and slow crack growth parameters for CVD silicon carbide. Specimens were cut from various locations in a 25 mm thick, 50 cm diameter piece of SiC to analyze bulk material property homogeneity. Flexural strength was measured using a four-point bend technique. In addition to mechanical testing for strength, hardness, and fracture toughness, the material crystallography and microstructure were studied. Thermal expansion, thermal diffusivity, specific heat, optical absorption, and infrared reflectivity measurements were also conducted. Raman spectroscopy was used to check for any residual stress. Test results show this CVD silicon carbide is a high-purity, homogeneous, fine-grained substrate material with very good mechanical, optical, and thermal properties.

14. SUBJECT TERMS
silicon carbide, material properties, Weibull analysis, mirror substrates, reflective optics

15. NUMBER OF PAGES
60

16. PRICE CODE

17. SECURITY CLASSIFICATION OF REPORT	18. SECURITY CLASSIFICATION OF THIS PAGE	19. SECURITY CLASSIFICATION OF ABSTRACT	20. LIMITATION OF ABSTRACT
UNCLASSIFIED	UNCLASSIFIED	UNCLASSIFIED	UL

ABSTRACT

Chemically vapor deposited (CVD) silicon carbide (SiC) is a serious candidate for the mirror substrate required for high-quality, reflective optics based on mechanical, optical, and thermal properties obtained from research quantities of material. Until recently, sufficient quantities of bulk material were not available for obtaining statistically valid quantities of data required for brittle material lifetime predictions.

The primary purpose of this material characterization study was to obtain sufficient mechanical property data for CVD SiC to determine the Weibull and slow crack growth parameters. Data was obtained on flexural strength (four-point bend) specimens taken from a bulk piece of material originally 0.5 m in diameter by approximately 25 mm thick. Specimens were cut from various locations within the material to allow for a statistical analysis to determine material property homogeneity throughout the bulk. In addition to the mechanical strength, crystallography, microstructure, fracture toughness, hardness, thermal expansion, thermal diffusivity, specific heat, optical absorption, and reflectivity were studied. Raman spectrographic analysis was also used to determine if residual stress was present in the bulk material.

The conclusions from this study were that chemical vapor deposited silicon carbide can be produced which is pure, homogeneous, fine grained material. The samples evaluated exhibited very good mechanical, optical, and thermal properties when compared to other materials being considered for optical substrates.

TABLE OF CONTENTS

TABLE OF CONTENTS (concluded)

LIST OF ILLUSTRATIONS

LIST OF TABLES

INTRODUCTION

OBJECTIVE

For several years Morton International (MI) was supported by the Air Force/SDIO to perform research and development of fabrication methods for preparing cubic (β) silicon carbide (SiC) by chemical vapor deposition (CVD) for optics applications. Earlier characterization of the material taken from various research fabrication processing runs indicated that the material had extremely high-purity, was very homogeneous, with high average strength and Young's modulus values for a polycrystalline ceramic material. During the development process, however, the results of various characterization studies were somewhat inconsistent, as MI worked to improve control over its process, while scaling equipment to fabricate 1.5 m diameter pieces up to 25 mm thick. There was an insufficient amount of material and inadequate funding available to prepare a statistically meaningful compilation of material property data. It became apparent during the final phase of the program that an extensive material characterization study, producing consistent, reliable values, would be necessary if designers were to have sufficient confidence in the lifetime predictions required for incorporating the material into their optical systems.

The objective of this program was to provide the required thermal, mechanical, and optical property data for SiC synthesized by the CVD process. This was necessary to establish a validated design guide for use of this material in critical optical/ structural applications. Major emphasis was placed on obtaining sufficient mechanical property data to determine Weibull and slow crack growth parameters. An analysis of variance (ANOVA) was also performed to determine if significant differences in mechanical strength existed in specimens obtained from different locations in the bulk material. The measurement of thermal properties, conductivity, diffusivity, specific heat, and coefficient of thermal expansion (CTE) as well as some optical properties were also performed.

The test matrix design for this study and the test procedures used to acquire the data were based on UDRI's past experience in dealing with lifetime predictions for brittle materials being used in structural applications.

APPROACH

The Government provided bulk CVD silicon carbide prepared by Morton International in sufficient amounts to conduct this study. The bulk material was representative of the best material prepared in an Air Force/SDIO-sponsored material development program at MI. That program demonstrated that careful control of CVD processing parameters produced material with reproducible mechanical and optical properties. UDRI verified this consistency

by choosing random samples of new material from the scaled-up process and comparing them with data taken from material made during the development phase. Both materials were made using identical techniques, the original material was made in small experimental furnaces where more precise control was possible.

BACKGROUND

Design engineers have long recognized the need for establishing statistically significant property values for structural material. Because of their ductility and associated plastic deformation, the prediction of failure of metals can be quite precise. On the other hand, ceramics typically do not exhibit ductile behavior and their mechanical failure is much less certain. Structures made of ceramics most often fail in tension at a flaw on the object's surface. Typically, the flaw is small and cannot be easily detected. The flaw tip is usually quite sharp (of atomic dimensions) and, unlike metals, does not blunt when put in tension due to the lack of plastic flow. Catastrophic failure occurs at stresses dependent on the statistical distribution of surface flaws; thus, the relative unpredictability of the failure conditions.

Regardless of their brittle behavior, ceramics have come to the foreground of materials research because of their unique properties. These include high specific stiffness, chemical stability in severe environments, strength retention at elevated temperatures, dimensional stability over large temperature excursions, a wide range of thermal properties, and in some materials, excellent optical properties over a wide spectral range.

Despite the lack of precision in predicting a ceramic object's mechanical strength, systems can be appropriately designed using these materials in structural applications. With a reliable property values established, designers can have a high degree of confidence that a ceramic component will survive in use. It is important that data collection be sufficiently complete to ensure a design based on the data is neither overly conservative or dangerously underdesigned.

TECHNICAL APPROACH

The primary goal of the program was to obtain sufficient mechanical property data for CVD SiC, to perform a meaningful analysis, and provide design engineers with the tools for lifetime prediction. Due to the variation of flaw sizes that lead to failure in a brittle material, statistical methods must be used to analyze mechanical property strength data. Acceptable methods have been found that use the Weibull distribution function as the basis for determining the statistical parameters required to predict the probability of failure for a brittle ceramic material. Over the past 20 years, several models using the Weibull parameters have been developed for use in designing structural optical components.

Weibull Analysis

The Weibull two-parameter statistical strength model is most often used to characterize the strength of brittle materials [1]. The probability, F, that a component or specimen will fail at a surface flaw is given by,

$$F = 1 - \exp\left\{ - \int \left[\frac{\sigma}{\sigma_0} \right]^{m\Delta} dS \right\} \qquad (1)$$

$$F = 0 \text{ for } \sigma \leq 0$$

Note: m = meters

m = Weibull modulus

where σ is the applied stress, σ_0 is the Weibull scale parameter, and *m* is the Weibull modulus. For this analysis it was assumed that principal stresses act independently and that failure can occur at applied stress levels approaching zero. The integration is carried out over the tensile surface since it is also assumed that the probability of a compressive failure is negligible [2]. It may be noted that the probability of survival, defined as the reliability, R, is equal to 1-F.

For this effort, the two-parameter Weibull model was used to characterize the surface strength of CVD SiC specimens evaluated using four-point bend flexure tests [3]. The probability that a flexure test specimen will survive a given maximum outer-fiber tensile stress, σ, is given by the reliability, R:

$$R = \exp\{ - [\sigma / \beta]^m \} \qquad (2)$$

where β is the Weibull test scale parameter characteristic of the surface strength of CVD SiC material.

The Weibull material scale parameter, $\sigma_{0(s)}$ which is a characteristic of the specimen material surface strength, can be determined from flexure test results as a function of the test scale parameter, β, and the modulus, *m*. $\sigma_{0(s)}$ is given by,

$$\sigma_{0(s)} = \beta \, S'^{(1/m)} \qquad (3)$$

The variable S' represents an equivalent surface area under uniform uniaxial tensile stress that would have the same reliability as a flexure specimen exposed to the same maximum stress. S' is given by the equation:

$$S' = l_g \{ w + [t /(m + 1)] \} k \qquad (4)$$

where l_g is the flexural specimen inner gage length, w is the specimen width, and t is the specimen thickness. The factor k accounts for the possibility of failures between the inner and outer gage points, and is given by,

$$k = [\, m + (L / l_g) \,] / [m + 1] \tag{5}$$

where L is the outer gage length.

When strength distributions based on experimental evaluation of the strength of brittle materials deviate from a Weibull distribution, such deviation may be due to the existence of more than one distribution of failure-initiating defects in the as-fabricated specimens.

The Weibull cumulative probability of failure, F = 1 - R, for a group of identical specimens tested under identical conditions can be evaluated through the use of a ranking estimator as a function of specimen strength. For this analysis effort the Median Rank Estimator was used [4]. For each data set the specimen strengths were ordered from weakest to strongest and the failure probability was determined for each specimen. The median rank estimator is

$$F = (n_i - 0.5) / N \tag{6}$$

where n_i is the rank of the ith specimen and N is the total number of specimens in the group.

The determination of the Weibull parameters was accomplished through a linear regression analysis based on the two-parameter Weibull distribution (Equation 1):

$$\log\{ -\ln(R) \} = \log\{ 1/\beta^m \} + m \log\{ \sigma \} \tag{7}$$

Equation (7) corresponds to the linear equation

$$Y = A + b X \tag{8}$$

where $Y = \log\{ -\ln(R) \}$, $A = \log\{ 1/\beta^m \}$, $b = m$, and $X = \log\{ \sigma \}$.

Slow Crack Growth and Minimum Time to Failure

Ceramic materials are also susceptible to delayed failure due to a phenomenon known as "slow crack growth." Failure results from stress-assisted growth of subcritical flaws to a critical size in the presence of moisture or other corrosive environments. The factors governing the rate of subcritical crack growth in a given environment must be determined before a relationship between applied stress and failure probability can be determined.

Tests on a number of brittle materials have demonstrated that the rate of crack growth increases as the water content of the environment increases [13]. The rate of crack growth has been demonstrated to exhibit a power-law relationship with the stress intensity level, K_I [5]:

$$v = v_0 \left(\frac{K_I}{K_{IC}}\right)^n = A K_I^n \qquad (9)$$

where $K_I = Y \sigma_a c^{0.5}$, n is the slow crack growth exponent, and v_0 and A are alternative second crack growth parameters.

Integration of Equation (9) yields a relationship that can be used to calculate the minimum time, t_{min}, that a specimen or component will survive when exposed to a constant maximum applied tensile stress, σ_a [2].

$$t_{min} = \left\{\frac{2}{(n-2) A Y^n \sigma_a^n}\right\} \left\{\frac{1}{c_i^{[(n-2)/2]}} - \frac{1}{c_f^{[(n-2)/2]}}\right\} \qquad (10)$$

This can be simplified to

$$t_{min} = \frac{2}{(n-2) A Y^2 \sigma_a^2 K_{Ii}^{(n-2)}} \qquad (11)$$

where the initial value of the stress intensity is given by

$$K_{Ii} = Y \sigma_a c_i^{0.5} \qquad (12)$$

The variable c_i is the size of the maximum flaw in the region of maximum stress, σ_a, when the component enters operation. The parameter c_f is the size of the largest flaw when $t = t_{min}$. Assuming that the part fails at $t = t_{min}$,

$$c_f = \left(\frac{K_{Ic}}{Y \sigma_a}\right)^2 \qquad (13)$$

Using the above relationships, the time to failure can be estimated for any applied stress and failure probability if the Weibull parameter *m*, σ_i, K_{Ic}, crack growth rate, n and B are known.

Past experience at UDRI has shown that n and B are best determined by using "dynamic fatigue" techniques (most economical relative to test time and material required). The material of interest is tested to obtain its inert strength at a very high loading rate in liquid nitrogen. Three or more loading rates, each separated by at least an order of magnitude, are then performed in a corrosive environment. Using a relationship between the applied stressing rates and the fracture stress, n and B can then be calculated.

Dynamic Fatigue Analysis of Slow Crack Growth Parameters

The minimum time to failure Equation (11) may be written in a simpler form using an alternative second slow crack growth parameter, B, which may be determined through a dynamic fatigue approach [6,7]:

$$t_{min} = B \frac{\sigma_i^{(n-2)}}{\sigma_a^n} \tag{14}$$

The intrinsic, fast-fracture (zero crack growth), strength of the component is σ_i and the alternative second slow crack growth parameter, B, is given by

$$B = \frac{2}{(n-2)\, A\, Y^2\, K_{Ic}^{(n-2)}} \tag{15}$$

The analytical basis for the dynamic fatigue approach is the crack growth rate power law relationship described in Equation (9). The integration of the crack growth rate equation is carried out with the assumption that the stress rate, $\dot{\sigma}$, is constant. With such an assumption,

$$\sigma_f^{(n+1)} = \dot{\sigma}\, B\, (n+1)\, \sigma_i^{(n-2)} \tag{16}$$

where σ_f is the failure stress of a specimen or part tested at a constant stress rate, $\dot{\sigma}$. Taking the natural logarithm of Equation (16) yields,

$$\ln(\sigma_f) = \frac{\ln\dot{\sigma}}{(n+1)} + \frac{\ln[\, B\,(n+1)\,] + (n-2)\ln(\sigma_i)}{(n+1)} \tag{17}$$

This may be linearized to,

$$\ln(\sigma_f) = a_1 \ln\dot{\sigma} + a_2 \tag{18}$$

where

$$a_1 = \frac{1}{(n+1)} \tag{19}$$

and

$$a_2 = \frac{\ln[\, B\,(n+1)\,] + (n-2)\ln(\sigma_i)}{(n+1)} \tag{20}$$

Flexure tests at two or more constant stress rates in a water environment, combined with knowledge of the intrinsic strength of the material, provides the basis for evaluation of the linear equation variables a_1 and a_2, and subsequently, for the slow crack growth parameters n and B. Because of the scatter in the strength of brittle materials it is necessary to employ strength values at equivalent reliability levels. The median strength (R = 0.5) for each constant rate group of specimens, as well as the median strength of the intrinsic strength group, provides a reliable basis for this calculation.

EXPERIMENTAL PROCEDURE

TEST MATRIX

The test matrix for this study was developed based on Weibull analysis of four-point flexure tests on 30 specimens and dynamic fatigue testing on 30 specimens at each of four loading rates (Table 1). Past experience has shown that a sample of 30 specimens is usually adequate to perform a Weibull analysis on data obtained from dense, well prepared, homogeneous, brittle materials. In this study extra specimens were prepared for each sample set to ensure that at least 30 specimens would be available for flexural strength tests when Weibull parameter determinations were required. If more than 30 specimens survived the cutting and finishing process, all the specimens were tested. As indicated in Figure 1, the odd numbered specimens were obtained from near the deposition surface (top) and the even numbered specimens were obtained from the substrate side of the bulk material. All of the specimens tested in this study were obtained from the locations shown in Figure 1.

Table 1. Number and Dimensions of Specimens Tested

	Specimen Number and Dimension
CTE (α_{CTE})	6 specimens (50 x 6.5 x 6.5 mm)
Reflectivity and Zygo	6 specimens (38 mm dia. x 6 mm thick)
Optical Absorption and TIS	6 specimens (38 mm dia. x 6 mm thick)
Thermal Diffusivity (α_{TD})	6 specimens (13 mm x 13 mm x 2.5 mm)
Specific Heat (Cp)	3 specimens (scrap material)
Density (ρ)	3 specimens (flexure specimens were used)
Flexural Strength (σ_{MOR})	total of 150 four-point bend specimens (50 mm x 4 mm x 3 mm) 30 specimens tested at -180°C 30 specimens tested at room temperature, 4 stressing rates (120) 4-point bend bars (50 mm x 4 mm x 3 mm)
Fracture Toughness (K_{Ic})	10 specimens (50 mm x 5 mm x 4 mm)
Young's Modulus and Poisson's Ratio	8 specimens (75 mm x 13 mm x 6.5 mm)
Microhardness (V_H)	used K_{Ic} specimens for this study
X-Ray Diffraction	5 specimens (broken MOR specimens were used)
Metallography	10 specimens (broken MOR specimens were used)

CVD SiC CHARACTERIZATION CUTTING DIAGRAM

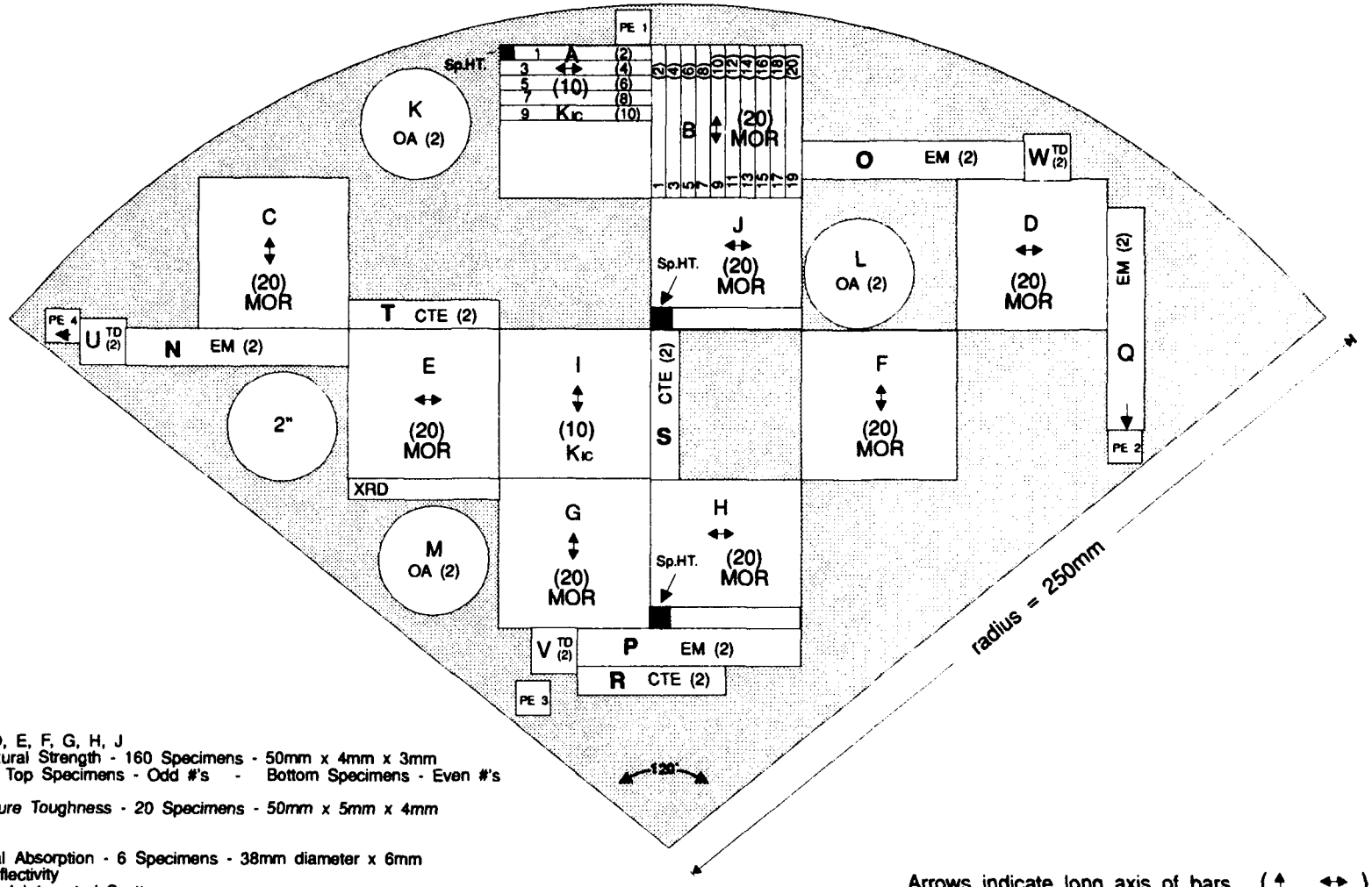

Figure 1. Bulk CVD SiC specimen cutting diagram.

SLABS - B, C, D, E, F, G, H, J
MOR - Flexural Strength - 160 Specimens - 50mm x 4mm x 3mm
Top Specimens - Odd #'s - Bottom Specimens - Even #'s

SLABS - A, I
K_{IC} - Fracture Toughness - 20 Specimens - 50mm x 5mm x 4mm

DISC - K, L, M
OA - Optical Absorption - 6 Specimens - 38mm diameter x 6mm
Reflectivity
Total Integrated Scatter

EM - Elastic Modulus - 8 Specimens - 75mm x 13mm x 6.5mm

CTE - Coefficient of Thermal Expansion - 6 Specimens - 50mm x 6.5mm x 6.5mm

TD - Thermal Diffusivity - 6 Specimens - 13mm x 13mm x 2.5mm

PE - Plasma Etch - 4 Specimens - Mounted

Sp. HT. - Specific Heat - 3 Specimens

Arrows indicate long axis of bars. (↕ ↔)

Slabs are approximately 13mm thick.

Not to Scale

MATERIAL

The bulk material used to prepare specimens was a pie-shaped (120° included angle) piece of chemically vapor deposited (CVD) silicon carbide (SiC) cut from a 0.5 mm diameter x 25 mm thick plate originally deposited by Morton International Inc. (MI), Woburn, MA. The final thickness of the piece was 16 mm; 8 mm was removed from the as-deposited side and 1 mm from the substrate side by diamond grinding. All of the rectangular specimens used in the study were cut from the bulk material as shown in the cutting diagram (Figure 1). A diamond cutoff saw,[1] using diamond embedded saw blades,[2] was used to cut the samples. The sample sides were ground flat and parallel with a grinding wheel[3] on the same machine. When available, four specimens from each group were selected for each set. Disk-shaped optical specimens were ultrasonically machined from the bulk material before being ground flat to within 1/10 λ and the edges beveled by Chan Kare Corp, Worchester, MA. Disk specimens were final polished to a surface roughness of approximately 3Å rms by Janos Corp, Townshend, VT.

X-RAY DIFFRACTION

Crystallographic studies were conducted with a Norelco x-ray diffractometer using Kα Cu radiation.

MECHANICAL PROPERTIES

Flexural Strength

Table 2 contains the actual number of test specimens used in this program and the test conditions for each group of specimens tested.

Table 2. Program Test Matrix for Mechanical Properties

Group	Number	Rate (m/s)	Environment
1	32	8.4×10^{-6}	liquid N_2
2	32	8.4×10^{-5}	distilled water
3	31	8.4×10^{-6}	distilled water
4	31	8.4×10^{-7}	distilled water
5	32	8.4×10^{-8}	distilled water

[1]Harig 618 slicer.
[2]Norton ASD120 R100B99, Norton Company, Worchester, MA.
[3]Radiac ASD 120R75.

The inert or fast fracture strength of CVD SiC was determined by four-point bend flexural tests conducted in a liquid nitrogen environment at a load displacement rate of 8.4×10^{-6}m/s (0.02 in/min), group 1 in Table 2. The conditions for the tests were chosen to minimize effects of slow crack growth and provide a sound basis for the determination of fast-fracture or inert-strength Weibull parameter values.

The inert strength flexural tests employed Size B specimens as identified in Mil-Std-1942A, 4 mm wide, 3 mm thick, with an outer span of 40 mm and an inner span of 20 mm. Uniform tensile stress loads were applied over the 20 mm span of the tensile surface of the specimens. A group of 32 specimens obtained from each MOR group (Figure 1) was tested.

Dynamic Fatigue

The dynamic fatigue measurements, groups 2 to 5 in Table 2, were taken using the same equipment, specimen preparation, and specimen size as group 1. Dynamic fatigue tests were conducted to obtain surface-flaw based, slow crack growth parameter values for CVD SiC. When possible, four specimens from each MOR group, two from the top and two from the bottom, were selected. The water environment provided a worst-case condition to assure that parameter values were conservative. The specimens were immersed in water contained in a plexiglass box resting on the testing machine platen.

Fracture Toughness

The fracture toughness (K_{Ic}) determinations were performed using a controlled flaw technique. A diamond Vickers indent was placed on the tensile surface of a flexure bar using a microhardness test apparatus.[4] A load sufficient to obtain cracks at the corners of the long diagonal of the indent was used. The length of the cracks were measured using low power optical microscopy. The specimens were then loaded to failure in a Universal testing machine[5]. The K_{Ic} value was determined using the following formula:

$$K_{Ic}^2 = 2.06\, \sigma_f (c/\pi)^{1/2} \qquad (24)$$

where σ_f = flexure strength (MPa)

c = radial crack extension (m)

[4]Zwicke Hardness 3212 Testing Machine, E. Windsor, CT

[5]Instron Model 1123, Instron Corp, Canton, MA

PHYSICAL PROPERTIES

Young's Modulus and Poisson's Ratio

A resonant frequency apparatus[6] was used to analyze the flexural and torsional vibrations on a 75 mm x 13 mm x 6 mm specimen after an impulse excitation. From these results the Young's modulus and Poisson's ratio are calculated.

Vickers Microhardness

Vickers hardness measurements were made using the microhardness tester[7] with a Vickers indenter. Measurements were obtained from the polished surface of fractured flexural strength test specimens using a 100 gm load.

THERMAL PROPERTIES

Coefficient of Thermal Expansion (CTE)

The coefficient of thermal expansion (CTE) measurements were obtained on a double rod quartz tube dilatometer[8] using a NIST 739-L1 fused silica standard.

Thermal Diffusivity

Thermal diffusivity measurements were carried out on a Xenon flash lamp apparatus. The frontface of a 13 mm x 2.5 mm specimen is irradiated with an energy pulse from the Xenon flashlamp. The resulting temperature profile is acquired on the back side and stored on a digital storage oscilloscope[9] for further analysis.

Specific Heat

Specific heat measurements were made on a differential scanning calorimeter[10] using sapphire as the reference material.

OPTICAL PROPERTIES

Calorimetry Measurement Apparatus

Absorptance of SiC was measured using laser rate calorimetry at $\lambda = 10.6$ mm. This consists of a source laser[11] operating single line at 10.6 μm, beam steering and alignment optics, a vacuum calorimeter chamber, and data collection apparatus. A 10.6 μm beam enters the

---

[6]Grindo Sonic, MK3, W. Lemmens Co., St. Louis, MO.
[7]Zwicke Model 3212 Hardness Testing Machine.
[8]Dilatronic Dilatometer, Theta Industries, Inc., Port Washington, NY.
[9]Nicolet Model 310 Digital Storage Scope.
[10]DuPont Instruments DSC2910, New Castle, PA.
[11]Coherent Model 41 CO_2

chamber through an AR coated window, strikes the sample, and is reflected back through the window and steered into a power meter.[12]

Temperature rise within the sample due to bulk absorption is monitored by two thermocouples separated diametrically by 180° which contact the sample side. Sensitivity is 80 μc/°C of temperature change. A nano-voltmeter[13] amplifies the signal and the data are recorded on an x-y recorder. Power reflected is also recorded.

Absorptance was measured at one location, the approximate center of the sample disc. The beam size was approximately 5-6 mm.

Spectral Reflectance Measurements

A Fourier transfer infrared spectrophotometer (FTIR)[14] was used to collect spectral reflectance survey scans from 2,500 to 25,000 nm on all of the samples. This instrument has a demonstrated precision of four decimal places; sufficient to clearly separate spectral differences between specimens.

Total Integrated Scatter (TIS)

TIS was measured at $\lambda = 0.6328$ μm. The apparatus used to determine the TIS is illustrated in Figure 2. The specimen is located near the midplane of a hemispherical collecting mirror commonly referred to as a Coblentz sphere. The radiation scattered from the specimen is imaged on a detector, and the reflected radiation is directed back through the center of the entrance hole in the sphere to an absorbing target. The circular entrance hole spans an angle of approximately 2.5°. The angle of incidence is maintained constant at 1° for all measurements. The radiation source is a HeNe laser operating at 633 nm. Rotating polarizers may be used for attenuating the laser beam, and apertures may be used to eliminate diffraction and extraneous scattered radiation. The Si detector output signal is measured with a suitable amplifier.

Raman Data Analysis

It has been well established that the width or the position of a Raman line can change due to strains introduced by either residual or applied stresses. The transverse optical mode (TO) Raman line at 795 cm^{-1} was recorded using a double spectrometer modified to use a liquid-nitrogen-cooled CCD array detector. The 795 cm^{-1} line is two-fold degenerate and has been observed to split with some specimens of cubic CVD SiC, presumably due to layering.

---

[12]Coherent Model 201
[13]Kiethley Model 148
[14]Nicolet Model 740

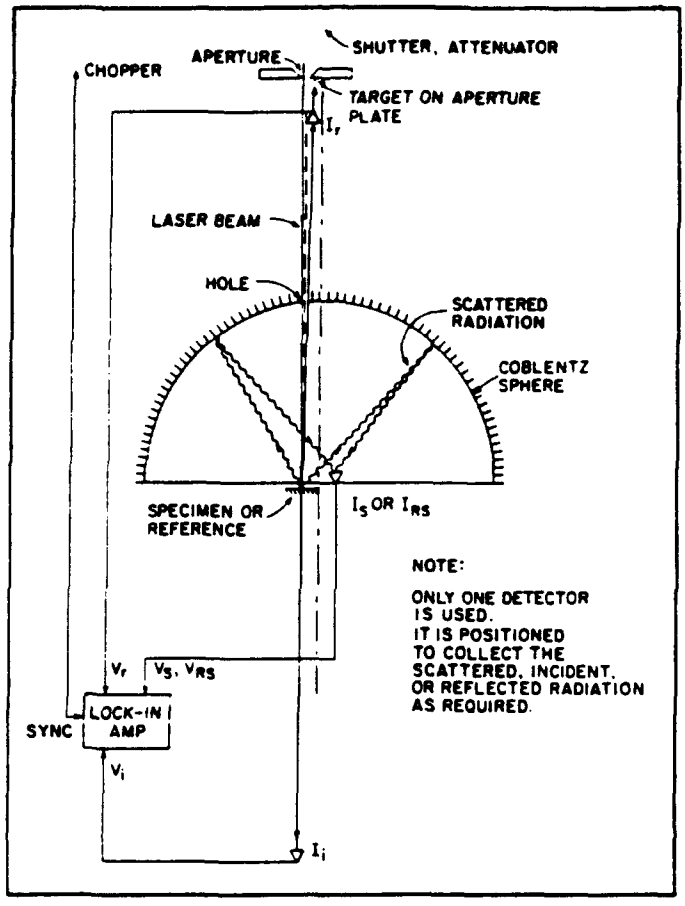

Figure 2. TIS measurement apparatus.

The specimens studied here showed no splitting. Therefore, the behavior of the full width at half maximum (FWHM) of the Raman line, which is generally sensitive to residual strain introduced by the fabrication process, was measured.

The laser spot size of the Raman microprobe dimensions for these studies was less than 2 microns wide by ~10 microns long. The narrow dimension was aligned parallel to the top-to-bottom direction to give high spatial resolution in the direction of translation. The laser was operated at 532 nm with less than 1 mW average power incident on the specimen. Spectrometer resolution was about two pixels or 0.7 cm^{-1} with the measured widths ranging from 2.8 to 4.7 cm^{-1}. All measurements were taken with the specimens at room temperature.

DISCUSSION OF RESULTS

The number of specimens prepared for testing and their dimensions are shown in Table 1. The specimen locations were selected from a variety of locations within the plate to provide information on the consistency of the material's mechanical properties. An analysis of variance was performed on the data to determine if a statistically significant difference existed in the mechanical properties of specimens taken from the various locations.

In this report any reference to the *substrate* side (bottom) of the bulk material is referring to the material deposited nearest the graphite substrate (initial material deposition). Reference to the *deposition* side (top) refers to the material nearest the final deposition surface.

In order to ascertain if CVD SiC from the large arc section used in this study was comparable to previously characterized material obtained from smaller furnaces, x-ray diffraction, and metallographic analyses were performed. These tests were used to determine crystal structure, possible preferred crystallographic orientation, grain size, void and/or inclusion content, and general surface conditions of polished specimens prior to further testing. Specimens for these studies were selected from various positions within the bulk material (Figure 1). Specimens also were prepared and tested to obtain thermal, optical, and physical properties from various positions in the bulk to further verify the homogeneity of the material.

The specific heat (Cp), coefficient of thermal expansion (CTE), thermal diffusivity (μ), density (ρ), and Vickers microhardness (VMH) were determined. Optical properties studied included total integrated scatter, absorption, and reflectance.

CRYSTALLOGRAPHY

X-ray diffraction results (Table 3) obtained from a specimen 16 mm thick indicated the material was β SiC (Figure 3) throughout the thickness. Minimal differences of intensity in the three orthogonal directions showed the amount of preferred orientation to be minimal even though the growth habit of the grains is "needle like." There was no indication of any hexagonal phases.

Table 3. X-ray Diffraction Results

SiC Side ⊥			SiC Bottom			SiC Top		
2θ	I	d (Å)	2θ	I	d	2θ	I	d
35.75	100	2.512	35.80	100	2.508	35.90	100	2.501
41.50	9	2.176	41.55	4	2.173	41.65	4	2.168
60.05	38	1.541	60.10	21	1.539	60.25	41	1.536

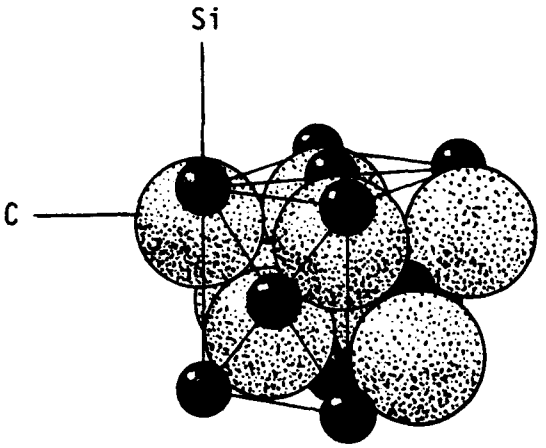

Figure 3. Schematic of β SiC crystallographic structure.

MICROSTRUCTURAL ANALYSIS

Micrographs of the as-received material are represented in Figures 4 through 6. These show typical microstructures observed on specimens taken from various locations in the bulk material.

Figure 4 shows the small grain size found on material deposited late in CVD deposition run. Much larger grains, shown in Figure 5, are a result of the bulk material being held at the deposition temperature for a long period of time (~72 hours). The typical elongated "needle like" CVD SiC grain structure in the plane of the growth direction is shown in Figure 6.

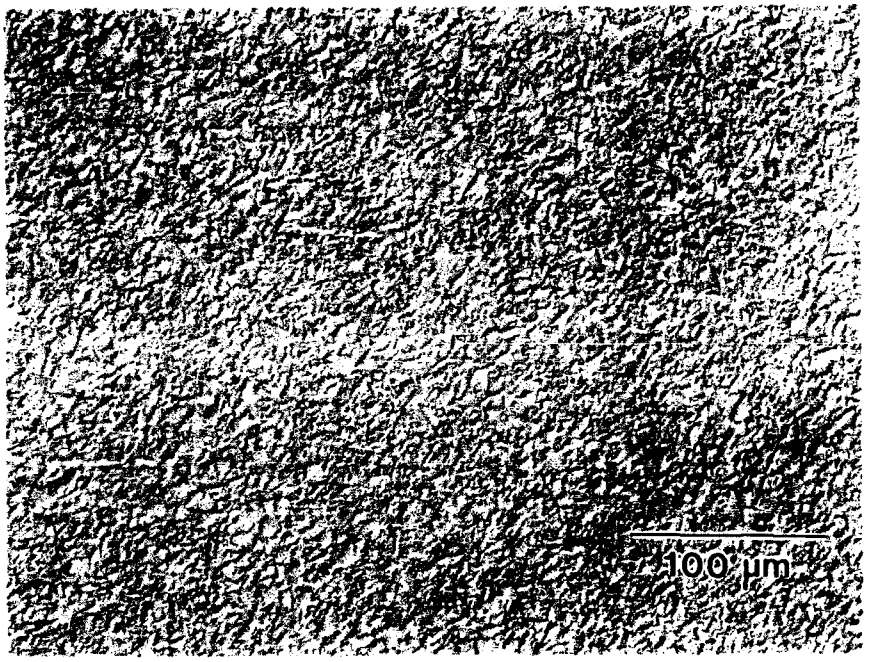

Figure 4. Microstructure of CVD SiC near deposition surface.

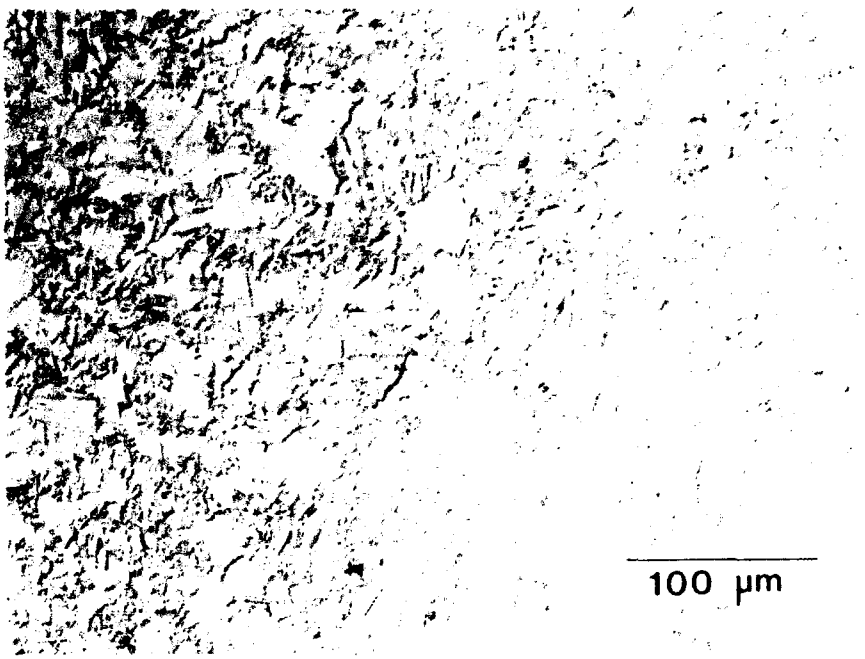

Figure 5. Microstructure of CVD SiC near substrate surface.

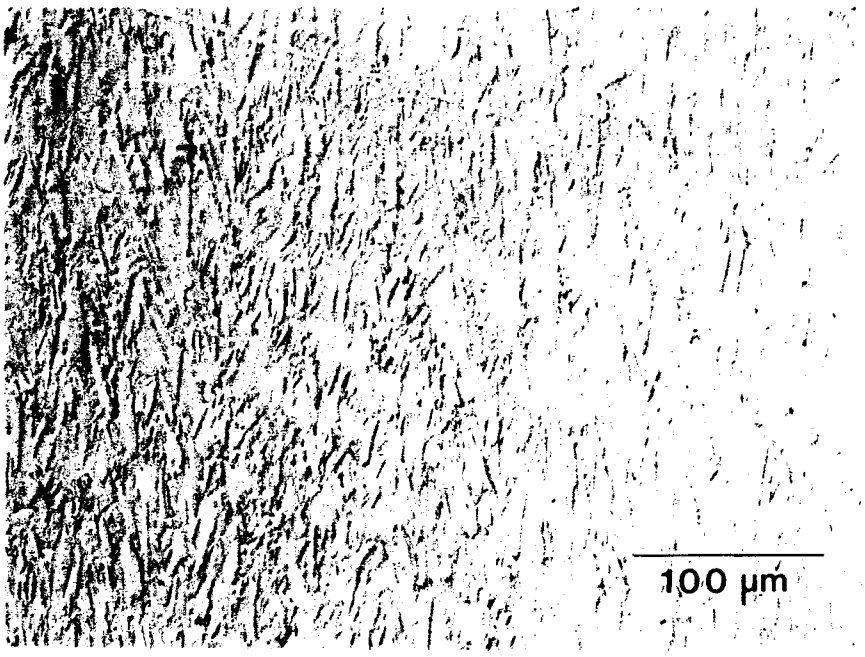

Figure 6. Microstructure of CVD SiC in the plane of the growth direction.

MECHANICAL PROPERTIES

Flexural Strength

Inert flexural strength values for specimens tested in liquid nitrogen at a loading rate of 8.4×10^{-6} m/s (0.02 in/min) are shown in Table 4. The results of the dynamic fatigue flexural strength testing in water, at four loading rates over four orders of magnitude, are shown in Tables 5 through 8.

Table 4. Flexural Strength Results for CVD SiC Tested in Liquid Nitrogen at a Loading Rate of 8.4×10^{-6} m/s (0.02 in/min)

	Flexural Strength	
Specimen Number	(ksi)	(MPa)
C-4	34	236
G-4	36	253
J-4	36	254
H-2	38	265
B-4	40	279
C-2	43	297
H-3	44	303
F-2	44	308
D-1	44	308
D-4	45	317
E-1	46	322
C-1	47	325
G-2	48	334
E-4	50	350
E-2	52	361
F-3	53	368
H-1	53	370
E-3	54	372
H-4	54	374
G-1	54	374
G-3	54	376
F-4	54	377
F-1	55	380
B-2	57	398
D-2	59	409
J-1	59	410
J-2	60	417
C-3	61	427
B-3	62	432
J-3	63	438
B-1	66	460
D-3	68	475
Average	51.5	355
Std. Dev.	9.1	62

Table 5. Flexural Strength Results for CVD SiC Tested in H_2O at a Loading Rate of 8.4×10^{-6} m/s (0.02 in/min)

	Flexural Strength	
Specimen Number	(ksi)	(MPa)
H-12	22.6	156
H-10	29.3	202
C-9	30.8	212
C-11	36.8	254
E-12	37.6	259
G-10	38.7	267
E-11	39.4	272
G-9	43.4	300
G-11	45.3	312
J-11	47.7	329
F-9	48.2	332
F-12	48.3	333
D-11	48.4	334
J-9	48.4	334
H-11	49.2	339
B-11	49.4	341
B-10	49.4	341
J-12	50.8	350
D-9	51.2	353
B-12	52.0	359
J-10	52.0	359
B-9	52.2	360
C-12	52.7	364
F-11	53.8	371
G-12	54.2	374
D-10	54.3	374
D-12	55.8	385
F-10	55.9	385
E-10	56.4	389
H-9	57.6	397
E-9	62.0	427
Average	47.5	328
Std. Dev.	8.9	62

Table 6. Flexural Strength Results for CVD SiC Tested in H_2O at a Loading Rate of 8.4×10^{-6} m/s (0.02 in/min)

	Flexural Strength	
Specimen Number	(ksi)	(MPa)
J-6	27	193
H-8	28	197
J-8	28	198
B-6	30	108
D-5	32	225
J-5	35	241
E-7	35	245
G-5	37	257
H-6	40	277
C-7	40	279
H-7	41	284
B-5	42	291
E-5	44	304
D-8	44	308
F-6	44	309
C-8	47	326
F-5	47	327
B-7	48	332
G-8	48	337
F-8	49	342
E-8	49	343
C-6	51	353
D-7	52	364
J-7	53	366
D-6	54	375
G-7	55	382
G-6	55	382
B-8	55	385
F-7	56	391
H-5	58	400
E-6	61	421
C-5	63	441
Average	45.7	315
Std. Dev.	10.0	0

Table 7. Flexural Strength Results for CVD SiC Tested in H_2O at a Loading Rate of 8.4×10^{-7} m/s (0.002 in/min)

	Flexural Strength	
Specimen Number	(ksi)	(MPa)
H-16	23	160
H-14	32	224
C-15	33	229
J-15	35	247
E-15	38	263
F-13	39	272
E-14	40	276
B-16	40	278
J-13	42	290
F-16	43	297
F-14	43	302
H-13	44	305
E-13	45	315
G-16	47	324
G-13	47	325
C-13	48	334
B-14	49	339
C-16	50	347
J-14	51	355
J-16	52	361
B-15	53	367
D-15	53	368
C-14	53	369
F-15	54	375
B-13	54	375
G-14	54	377
D-13	55	384
D-14	56	386
D-16	57	398
G-15	57	399
E-16	59	410
H-15	59	413
Average	47.4	327
Std. Dev.	8.9	61

Table 8. Flexural Strength Results for CVD SiC Tested in H_2O at a Loading Rate of 8.4×10^{-8} m/s (0.0002 in/min)

	Flexural Strength	
Specimen Number	(ksi)	(MPa)
H-18	20	141
H-20	23	158
J-17	32	222
F-19	33	233
G-19	36	251
E-19	37	261
F-17	42	291
B-17	42	296
C-20	43	298
E-17	44	305
B-18	44	307
E-20	44	309
J-19	44	310
F-20	45	315
B-20	45	315
F-18	47	326
D-18	47	327
G-18	47	328
G-17	47	328
D-19	49	339
E-18	49	340
C-19	49	340
G-20	50	347
J-18	50	349
J-20	50	351
C-17	51	354
D-20	52	365
H-19	54	375
D-17	55	384
H-17	57	395
C-18	61	421
Average	45.3	312
Std. Dev.	9.0	62

Although the average strength results are lower than previously tested CVD SiC depositing runs, the strengths obtained are still quite high for monolithic ceramics. The lower strengths may be due to the larger than usual grains resulting from the longer CVD deposition times for this deposit which is 4-10 times thicker than previous MI CVD material tested at UDRI.

Inert-Strength Weibull Parameters

The linear regression relationship employed to evaluate the inert strength Weibull parameters is illustrated in Figure 7, and the corresponding Weibull failure probability versus failure stress is plotted in Figure 8.

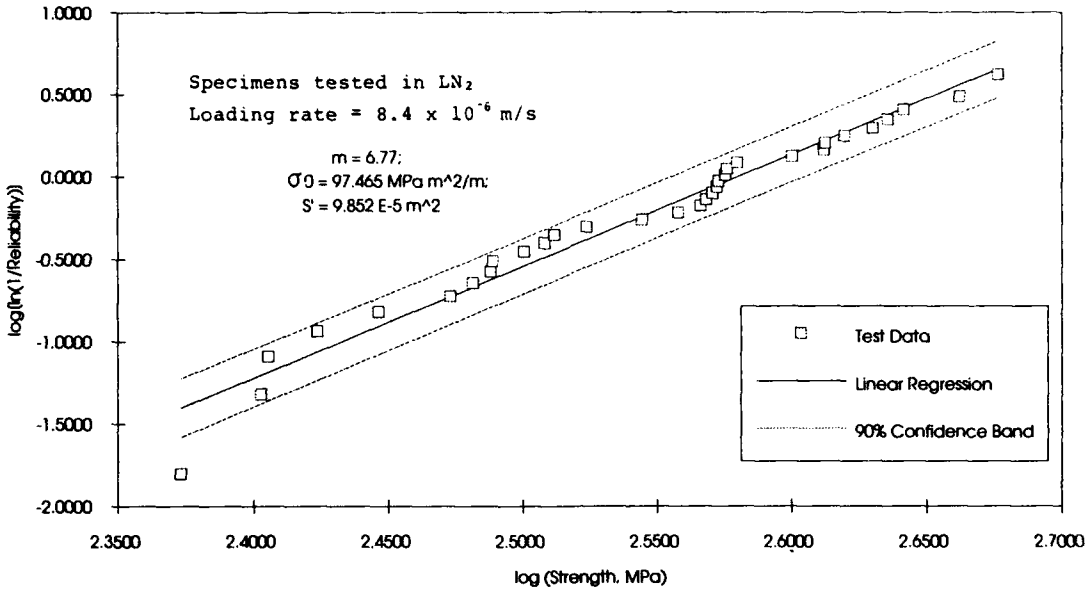

Figure 7. Linear regression fit of Weibull flexural test data.

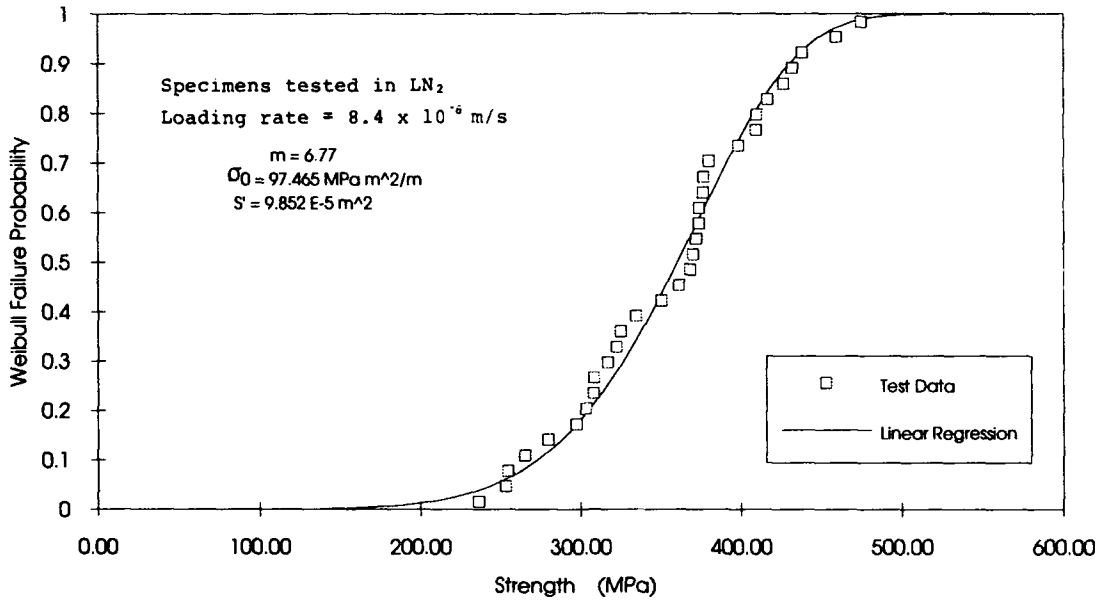

Figure 8. Weibull failure probability versus strength plot of flexural specimens tested in liquid nitrogen.

The results of the Weibull inert surface strength evaluation are:

Weibull Modulus, m: 6.77
Weibull Scale Parameter, σ_0: 97.46 MPa $m^{(2/m)}$
Average Strength: 355.2 MPa
Weibull-Based Median Strength: 360.4 MPa

Slow Crack Growth

The linear relationship between ln(stress rate) and ln(median strength) employed by the dynamic fatigue approach to evaluate the slow crack growth parameters is illustrated in Figure 9. The results of the Weibull analysis of all flexure tests listed in Table 2 are summarized in Table 9.

The results of the dynamic fatigue evaluation of slow crack growth parameters for CVD SiC Size B Flexure specimens are:

Slow Crack Growth Exponent, n: 216
Slow Crack Growth Parameter, B: 7.88E-6 sec MPa^2.

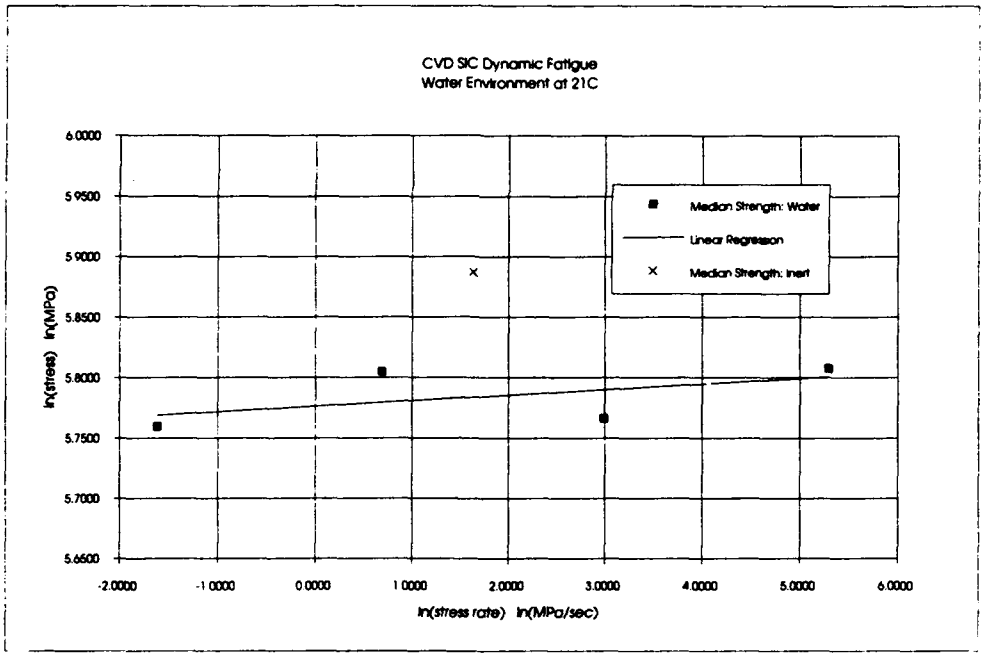

DYNAMIC FATIGUE ANALYSIS FOR CVD SiC SIZE "B" FLEXURE SPECIMENS

Displacement Rate	Stress Rate	Median Strength sig_med	Calculated Median Strength sig_med	ln(Stress Rate)	ln(Median Strength)	Calculated ln(Median Strength)
cm/min	MPa/sec	MPa	MPa	ln(MPa/s)	ln(MPa)	ln(MPa)
Water						
5.08E-04	1.99E-01	317	320	-1.6147	5.7586	5.7667
5.08E-03	1.99E+00	332	324	0.6879	5.8049	5.7793
5.08E-02	1.99E+01	319	327	2.9905	5.7662	5.7900
5.08E-01	1.99E+02	333	330	5.2931	5.8079	5.8006
Inert						
5.08E-02	5.13E+00	360	325	1.6349	5.8871	5.7837

LINEAR RELATIONSHIP
ln(median strength) = a1 [ln(stress rate)] + a2
a1 = 0.004616
a2 = 5.7782
CRACK GROWTH EXPONENT, n:
n = (1 / a1) - 1
n = 216
CRACK GROWTH PARAMETER, B:
B = (exp[(a2 /a1) - (1/a1 - 3) * ln(sig_med)]) * a1
B = 7.88E-06 sec^MPa^2
ALTERNATE CRACK GROWTH PARAMETERS:
v0 = 2 Klc^2 / [B Y^2 (n-2)]
Y = 1.264; Klc = 0.6 MPa m^.5
v0 = 4.65E+03 m/sec
A = v0 / Klc^n; log(v0) = log A + n log(Klc)
log A = -82.14 log(m/s MPa m^.5)

Figure 9. Dynamic fatigue results for CVD SiC.

Table 9. CVD SiC Flexure Test and Weibull Analysis Results

CVD SiC FOUR-POINT BEND FLEXURE SPECIMENS, SIZE B, 3mm x 4mm x 50mm						
Displacement Rate	cm/min	5.08E-02	5.08E-01	5.08E-02	5.08E-03	5.08E-04
Test Envrionment		Liq.N_2	Water	Water	Water	Water
Test Purpose		Inert	Dyn.Fat	Dyn.Fat	Dyn.Fat	Dyn.Fat
Weibull Modulus		6.77	5.53	5.26	5.90	5.08
Weibull Scale Parameter	MPa*m^(2/m)	97.46	67.52	59.78	74.31	56.05
Flexure Bar Median Strength	MPa	360.3	332.9	319.4	331.9	317.2
Average Strength	MPa	355.3	327.8	315.2	327.2	312.3
Effective Surface Area, S'	m^2	9.85E-05	1.02E-04	1.03E-04	1.01E-04	1.04E-04
Average Stress Rate	MPa/sec	5.13E+00	1.99E+02	1.99E+01	1.99E+00	1.99E-01
Number of Specimens Tested		32	31	32	32	31

Inspection of Figure 9 indicates that the slope of the plotted line is very close to zero which indicates that CVD SiC is not subject to slow crack growth. The results of this evaluation indicate that CVD SiC exhibits a negligible propensity for slow crack growth. Results of dynamic fatigue flexure tests show that the stress rate has very little effect on the median strength of the four test groups.

PHYSICAL PROPERTIES

Young's Modulus and Poisson's Ratio

The results of the resonant frequency room-temperature Young's modulus determinations, obtained from eight specimens, taken from various locations (Figure 1) within the bulk material, are shown in Table 10. These results are typical of homogeneous, pore-free CVD SiC. They are among the highest values ever recorded for polycrystalline SiC.

Table 10. CVD SiC Young's Modulus as Determined by Resonant Frequency Technique

Nearest Surface	Locations (see Figure 1)	Young's Modulus GPa (x10^6 psi)
Deposition Surface	Location N	460.9 (66.9)
Substrate Surface	Location N	461.5 (67.0)
Deposition Surface	Location O	464.1 (67.4)
Substrate Surface	Location O	460.5 (66.8)
Deposition Surface	Location P	461.7 (67.0)
Substrate Surface	Location P	462.0 (67.1)
Deposition Surface	Location Q	463.7 (67.3)
Substrate Surface	Location Q	461.6 (67.0)

Fracture Toughness

The fracture toughness (K_{Ic}) values for 10 specimens is given in Table 11. These values are typical for CVD SiC material obtained from MI during the development program.

Table 11. Fracture Toughness (K_{Ic}) Results Obtained by the Controlled Flaw Technique

Specimen Number	Average Crack Extension (μm)	Fracture Toughness (MPa $m^{1/2}$)
A-1	87.5	2.5
A-2	71.5	2.5
A-3	83.0	2.2
A-4	97.5	2.5
A-5	67.5	2.1
A-6	97.5	2.6
A-7	77.0	2.4
A-8	63.0	2.3
A-9	55.0	2.1
A-10	98.5	2.5
I-1	81.8	2.8
I-2	97.0	2.6
I-4	90.0	2.5
I-5	102.0	2.5
I-6	101.5	2.5
I-7	94.0	2.7
I-9	98.8	2.2
I-10	108.5	2.6

Microhardness

Results of the Vickers Microhardness tests are found in Table 12.

Table 12. Microhardness of CVD SiC

Test Temperature: 70°F (21°C) Crosshead Speed: 8.4×10^{-6} m/s (0.02 in/min) Relative Humidity: 55%	Average Standard Dev.	2.4 0.2
Indenter Load Used: 100 g	Spec. No.	Vickers Hardness (kg/mm)
	A1	2264
	A3	2083
	A7	2241
	I2	2231
	I8	2174
		Avg. 2199

THERMAL PROPERTIES

Coefficient of Thermal Expansion (CTE)

The results of the CTE analysis, over various temperature ranges, obtained from six specimens are given in Table 13. A least squares fit of the data for the six specimens is shown in Figure 10.

Table 13. CVD SiC Thermal Expansion (CTE)

Temperature Range (°C)	Coefficient of Thermal Expansion (mm/mm/°C) Top - deposition surface; Bottom - substrate surface					
	R-Top	R-Bottom	S-Top	S-Bottom	T-Top	T-Bottom
-150 to -100	0.53	0.55	0.44	0.64	0.42	0.43
-100 to -50	1.08	1.09	0.94	1.15	1.01	0.98
-50 to 0	1.66	1.67	1.50	1.69	1.55	1.56
0 to 50	2.09	2.17	2.02	2.20	1.98	1.90
5o to 100	2.59	2.62	2.53	2.67	2.53	2.48
100 to 150	3.15	3.06	3.05	3.03	2.99	2.95
150 to 200	3.28	3.45	3.48	3.43	3.43	3.45
200 to 250	3.67	3.67	3.81	3.66	3.75	3.78
250 to 300	3.97	4.02	4.12	4.01	4.07	4.08

Heating Rate: 300°C/hour
Atmosphere: Air
Reference: Fused Silica

Thermal Diffusivity

The thermal diffusivity values over the temperature range 21°C to -175°C is given in Table 14 for the six specimens measured. The reason for the low values obtained from the U-Top specimen are unknown. The specimen was retested with the same results (within experimental error).

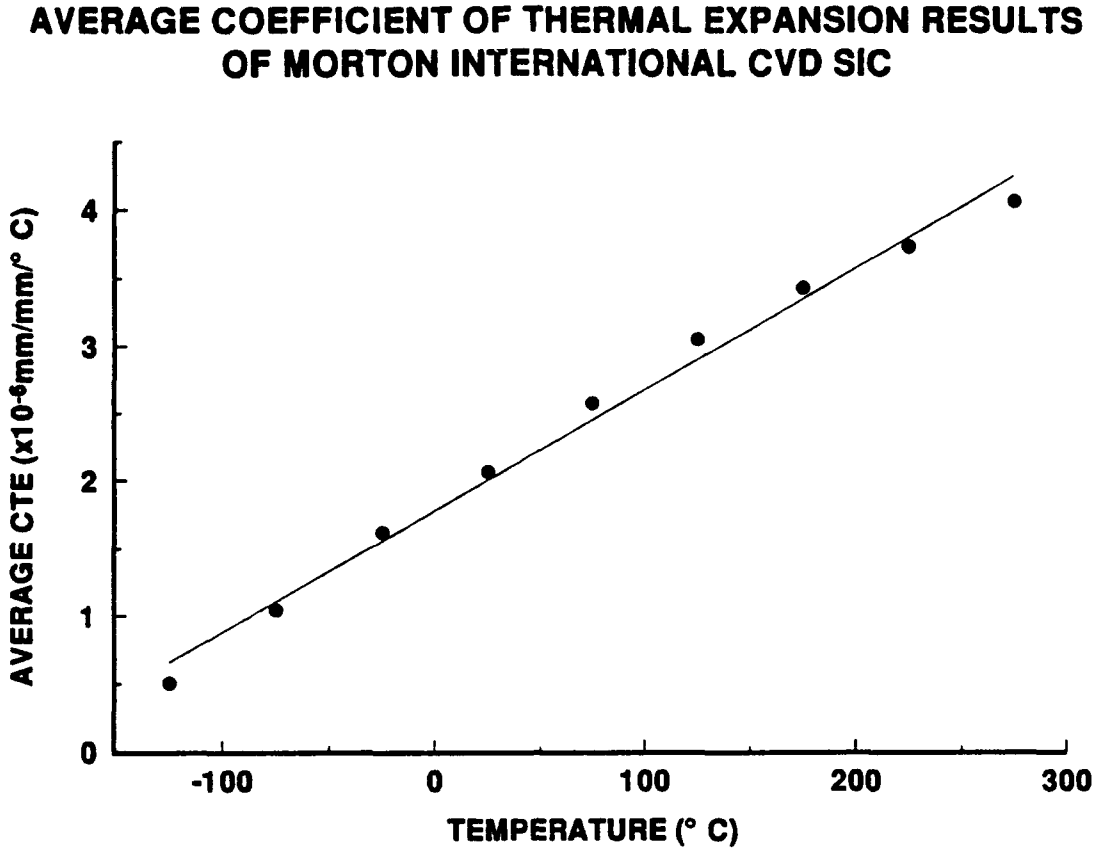

Figure 10. Least squares fit of CTE data.

Table 14. Thermal Diffusivity Obtained from Bulk Material (Top and Bottom), at Locations U, V, and W.

Test Temperature	Thermal Diffusivity (cm^2/sec) Top - deposition surface; Bottom - substrate surface					
°C	U-Top	U-Bottom	V-Top	V-Bottom	W-Top	W-Bottom
21	0.635	1.082	1.004	1.076	0.963	1.148
-25	0.787	1.529	1.321	1.404	1.339	1.455
-75	1.019	2.275	1.836	1.891	1.824	2.032
-125	1.384	3.175	2.449	2.664	2.386	2.893
-175	1.847	No Data	3.550	No Data	3.118	3.986

Note: An Armco Iron standard was run before each set of tests. The Armco Iron standard test results were adjusted, using a correction factor, to a thermal diffusivity of 0.202 cm^2/s. This factor was then used to correct the test data.

Specific Heat

A plot of the specific heat from -140°C to 600°C is shown in Figure 11. The plotted data are the average values of three differential scanning calorimetry (DSC) measurements obtained from three specimens.

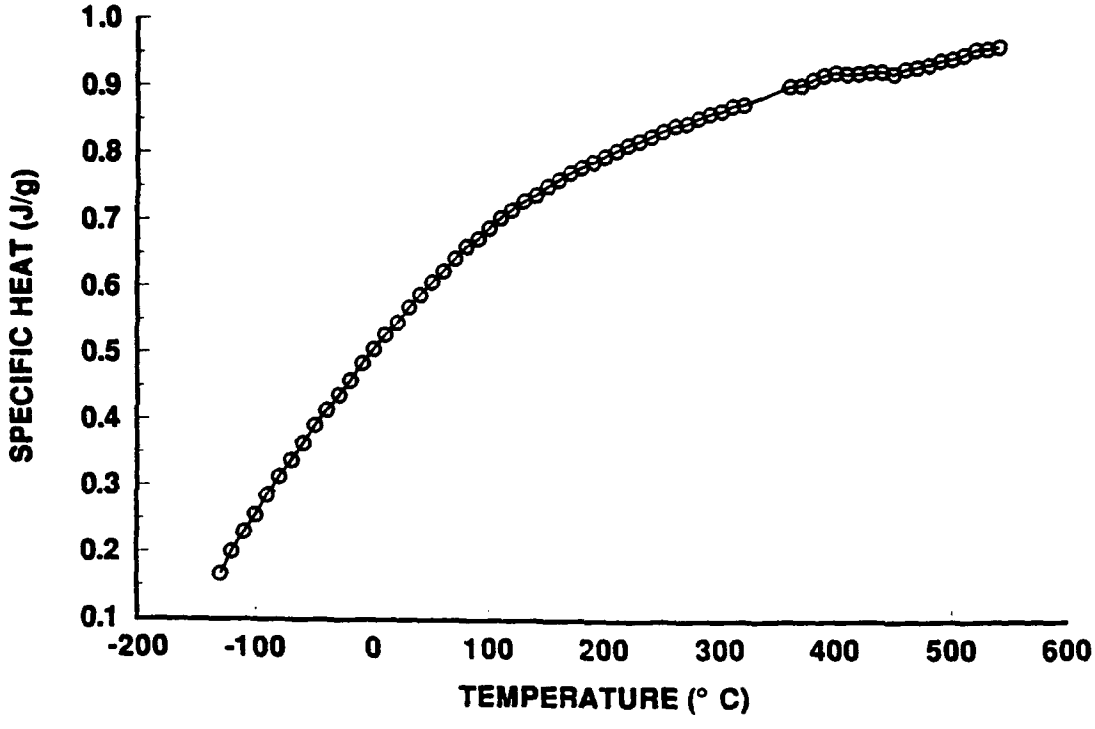

Figure 11. Plot of the specific heat results for CVD SiC.

OPTICAL PROPERTIES

Absorption Measurement Data Reduction

Measurement of optical absorption was accomplished using laser rate calorimetry which is the most sensitive and most accurate (±15%) conventional technique. Precision of the measurement as related from sample to sample variations and measurement repeatability is better than ± 0.0005 for the specimens tested.

Table 15 summarizes the values of absorptance (P_a/P_r)measured. Each column represents a remounting and re-measurement of the absorption.

Table 15. CVD SiC Optical Absorption Results for $\lambda = 10.6$ μm

Specimen Location	Absorptance (Pa/PR)				
No.	10^{-1}	10^{-1}	10^{-1}	10^{-1}	Mean x 10^{-1}
L-top SN 1	1.26	1.30	Aleonox Cleaned 1.20		1.25 ± .05
L-bottom SN 2	1.28	1.29	1.28		1.28 ± .006
K-top SN 3	1.15	1.15			1.15 ± .0003
K-bottom SN 4	1.16	1.16			1.16 ± .0007
M-top SN 5	1.30	1.32	1.32	1.30	1.31 ± .01
M-bottom SN 6	1.29	1.28	1.25		1.27 ± .02

The absorption data fall into two statistically significant groups. Four specimens group about the 0.1278 ± 0.025 absorptance value. The other two specimens average absorptance is 0.1155 ± 0.007. Repeated measurements confirmed the accuracy of these values.

Reflectance Measurement Results

Reflectance of all samples was measured between 2,500 to 25,000 nanometers using a bare gold mirror for reference. This technique did not yield absolute reflectance values but did yield highly accurate relative reflectance values.

One representative sample from the absorptance group is shown in Figure 12. No attempt was made to analyze the data, however, there was indication of a slight broadening of the reflectance peak in the 10.6 μm area for the samples with lower absorptance.

Total Integrated Scatter

Measurement of the surface finish of optical components is of considerable interest in assessing the quality of the components and predicting their performance. The measurement of total integrated scatter (TIS) provides a method of quantifying surface micro-roughness. TIS is related to the rms surface roughness for whose topography surfaces satisfy certain statistical criteria with respect to the randomness of the amplitudes and the spatial frequency distribution of defects. Table 16 summarizes the results of the measurements made on the six silicon carbide specimens identified for the TIS measurements and calculated values of hrms (Figure 1).

Janos Corp. reported surface roughness, measured by contact profilometry, to be better than 3Å rms on all six specimens.

Table 16. CVD SiC Total Integrated Scatter (TIS) Results for $\lambda = 0.6328\ \mu m$

Specimen Number	TIS ($x10^{-4}$)	hrms (Å)
SN-1	6.10	12.2
SN-2	8.17	14.4
SN-3	4.92	11.1
SN-4	4.14	10.2
SN-5	4.01	10.1
SN-6	9.91	15.7

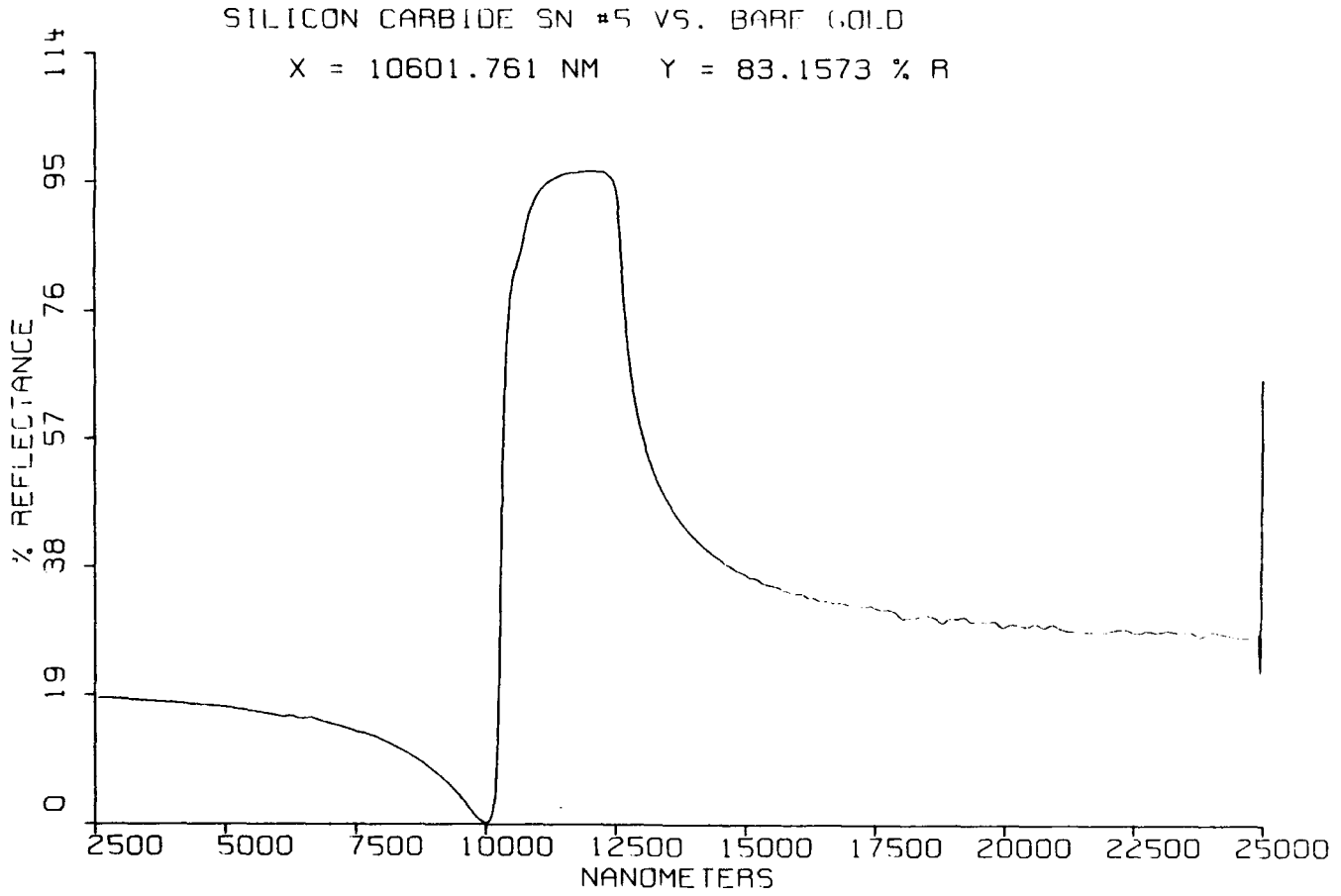

Figure 12. Typical reflectivity curve for CVD SiC.

Raman Microprobe Measurements

Three series of spectral measurements of the full width at half maximum (FWHM) of the 795 cm^{-1} Raman line were made to determine residual stress in the specimen. Figure 13 is a schematic of the Raman specimen indicating its orientation in the initial CVD material and the processing of the surfaces. The first series shown in Figure 14 (i.e., the chamfer) was across the side (plane of growth direction) from the deposition (top) surface in 10 μm steps, down the bevel and onto the side of the specimen towards the substrate surface (bottom). In the plane of the side, the bevel was determined to be 180 μm wide. The second series given in Figure 15 was again across the side of the specimen from the top to the bottom, except that the first four steps were at 50 μm intervals, the fifth step 400 μm from the top and the remaining four steps at 1000 μm (i.e., 1 mm) intervals. At the first six positions from the top, two measurements were made at different lateral locations to characterize the variations at the same transverse position. The third series across the end of the specimen, also in Figure 15, consisted of the first step at the top surface, two steps at 50 μm intervals followed by a step at 500 microns, with the remaining four steps at 1000 micron intervals towards the bottom surface.

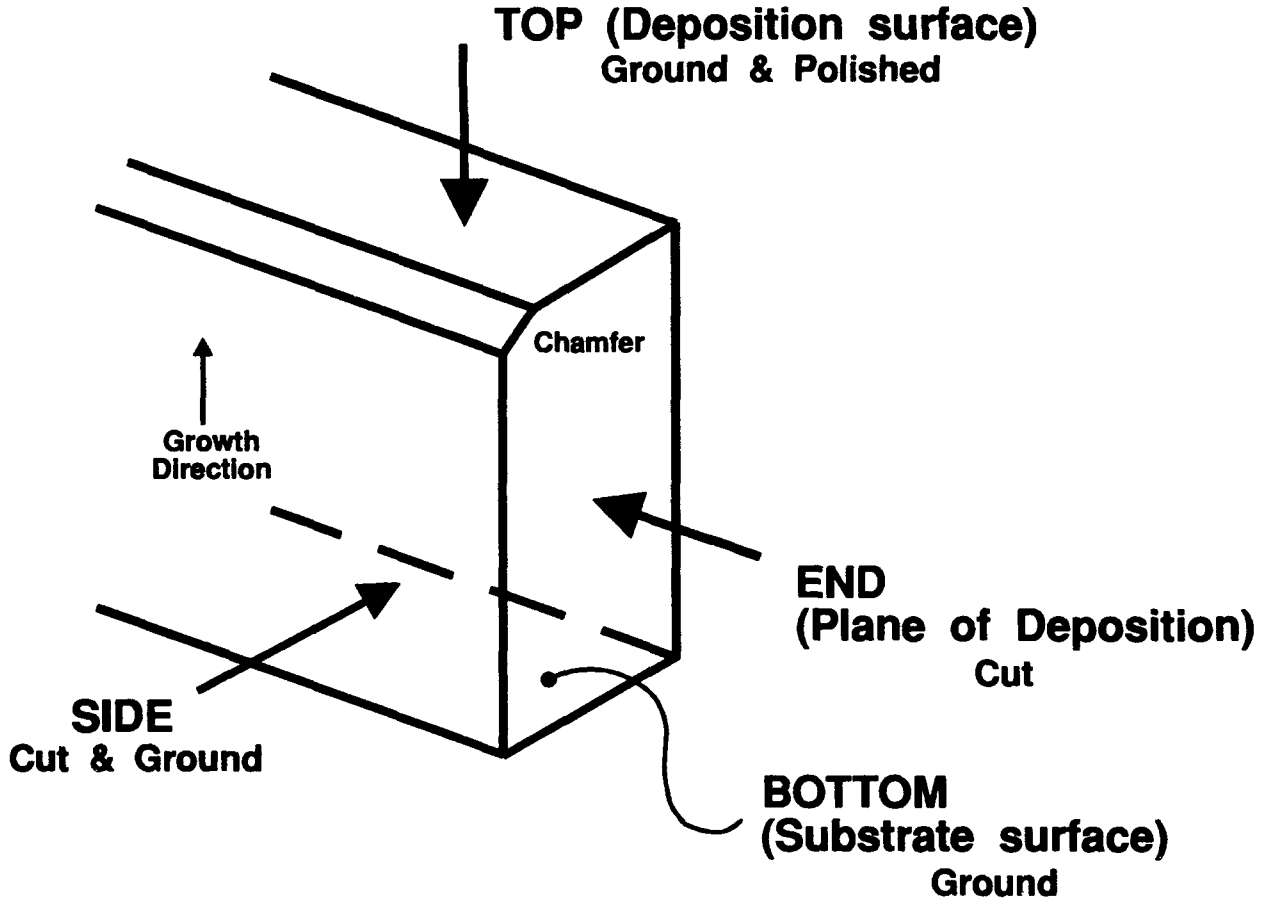

Figure 13. Diagram of Raman microprobe specimen.

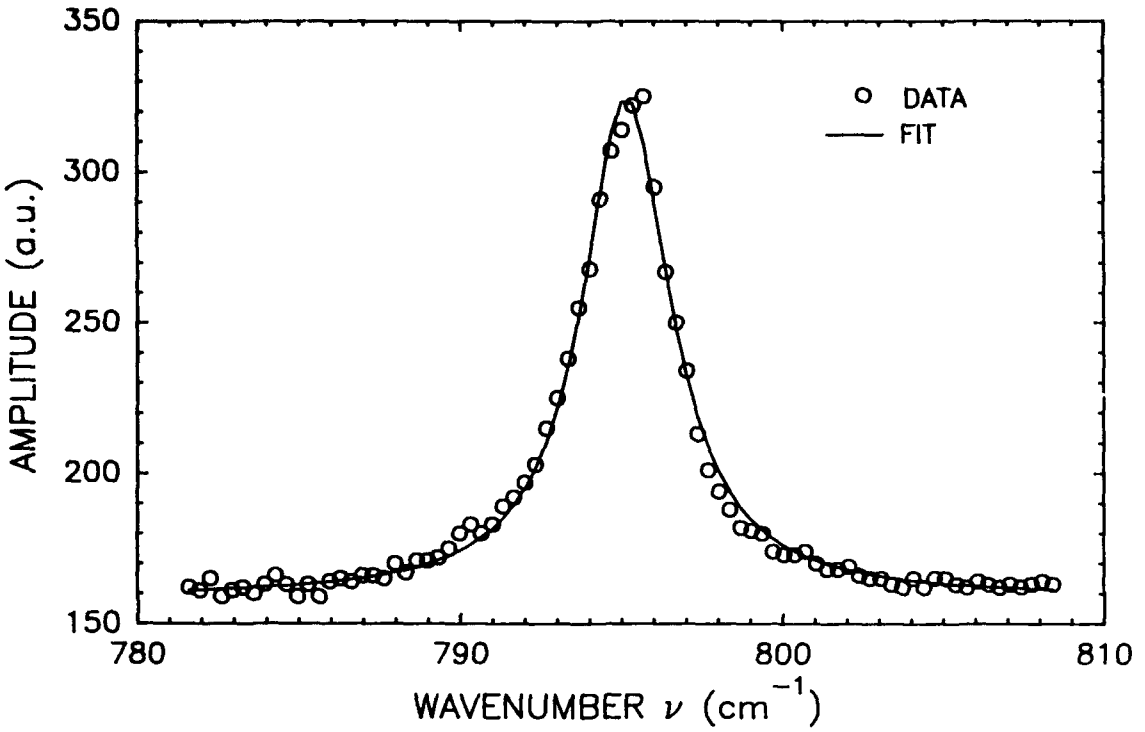

LORENTZIAN FIT: Amp=166±1%, ν_0=795.15±0.002%, FWHM=3.34±1.9%, Back=158.7±0.4%

Figure 14. Raman spectral line broadening due to residual strain on the side of the specimen that had been cut, ground, and beveled (i.e., chamfered).

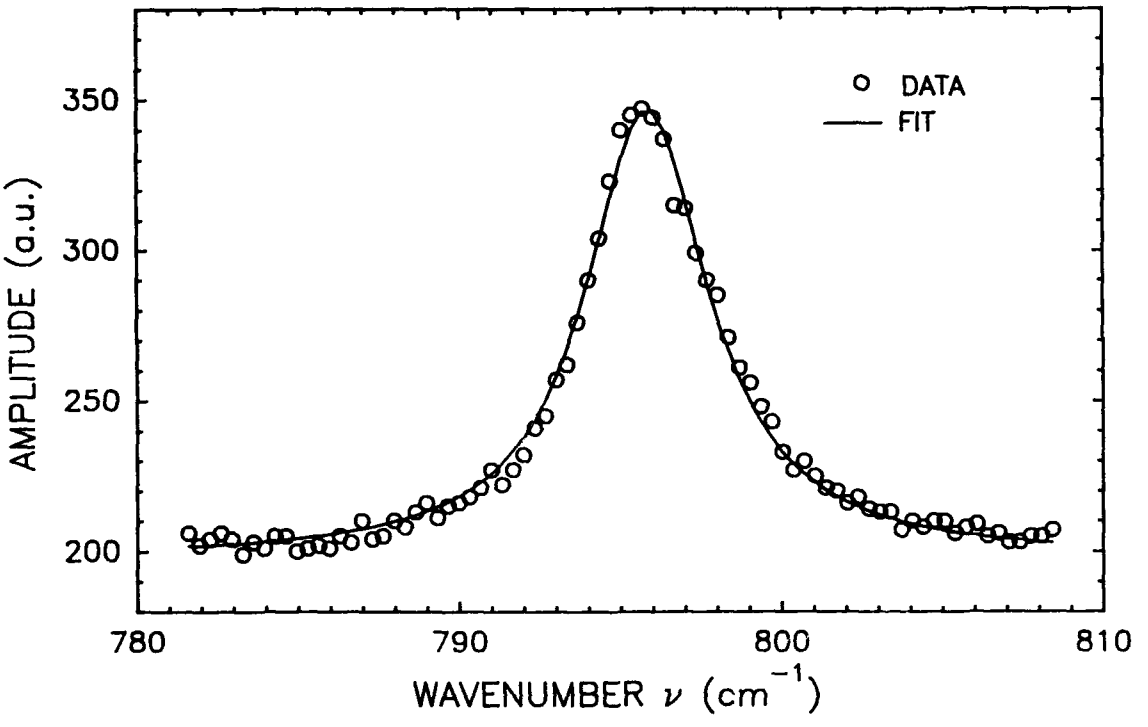

LORENTZIAN FIT: Amp=149±0.9%, ν_0=795.83±0.003%, FWHM=4.68±2.1%, Back=197.7±0.4%

Figure 15. Raman line broadening due to residual strain on end and side of specimen.

Data reduction was accomplished by a least squares fit of the Lorentzian line shape function. For each data set, the peak height above background, the line center position, the FWHM, and the background level were fit as free parameters. Three examples of the spectra are included (Figures 16 through 18), the solid curve is the fitted function and the data are given

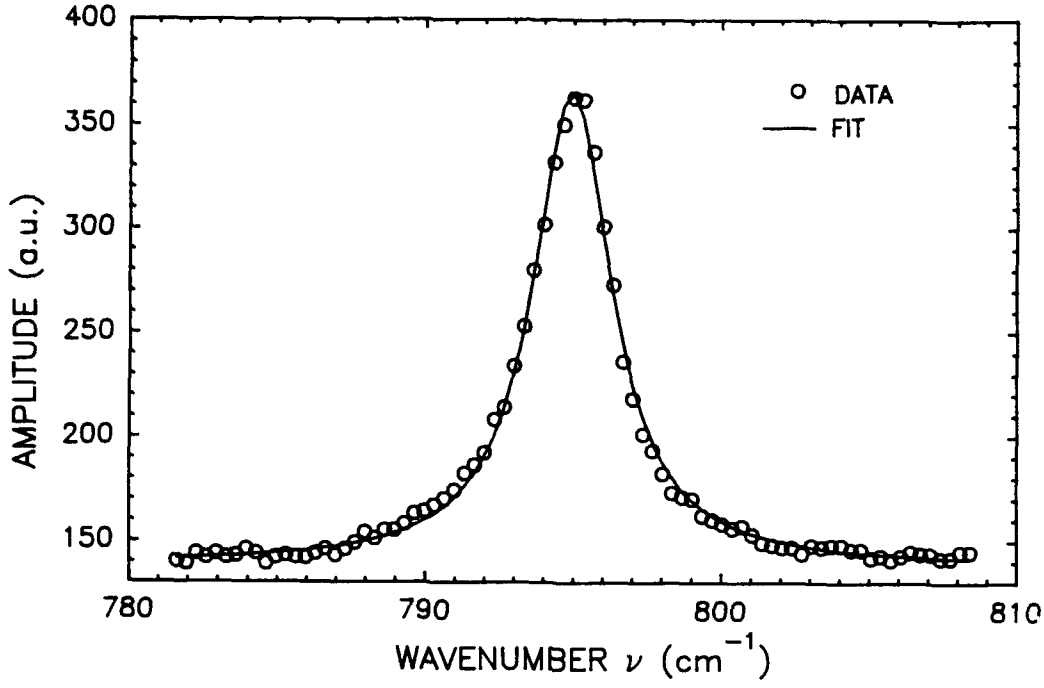

LORENTZIAN FIT: Amp=227±0.9%, ν_0=794.95±0.002%, FWHM=3.23±1.5%, Back=138.3±0.4%

Figure 16. Raman scan on the bevel of the cut and ground side 150 μm from the growth surface.

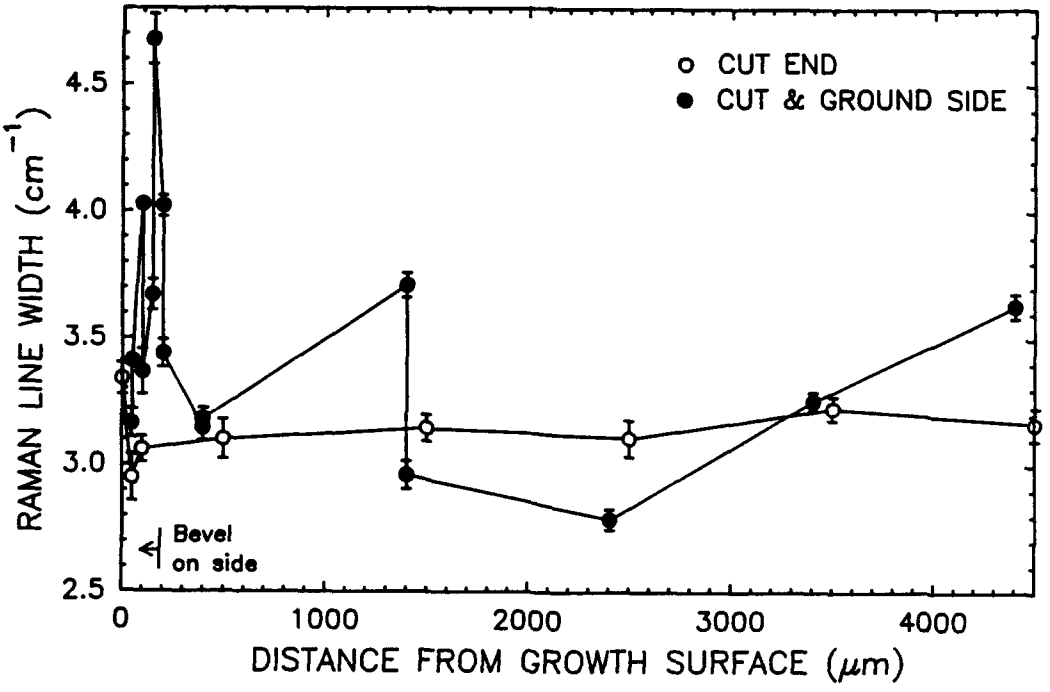

At each position, thru 1400 μm along the side of the specimen, two measurements were made at different lateral positions.

Figure 17. Raman scan on the diamond cut end at the growth surface (0 μm) of the specimen.

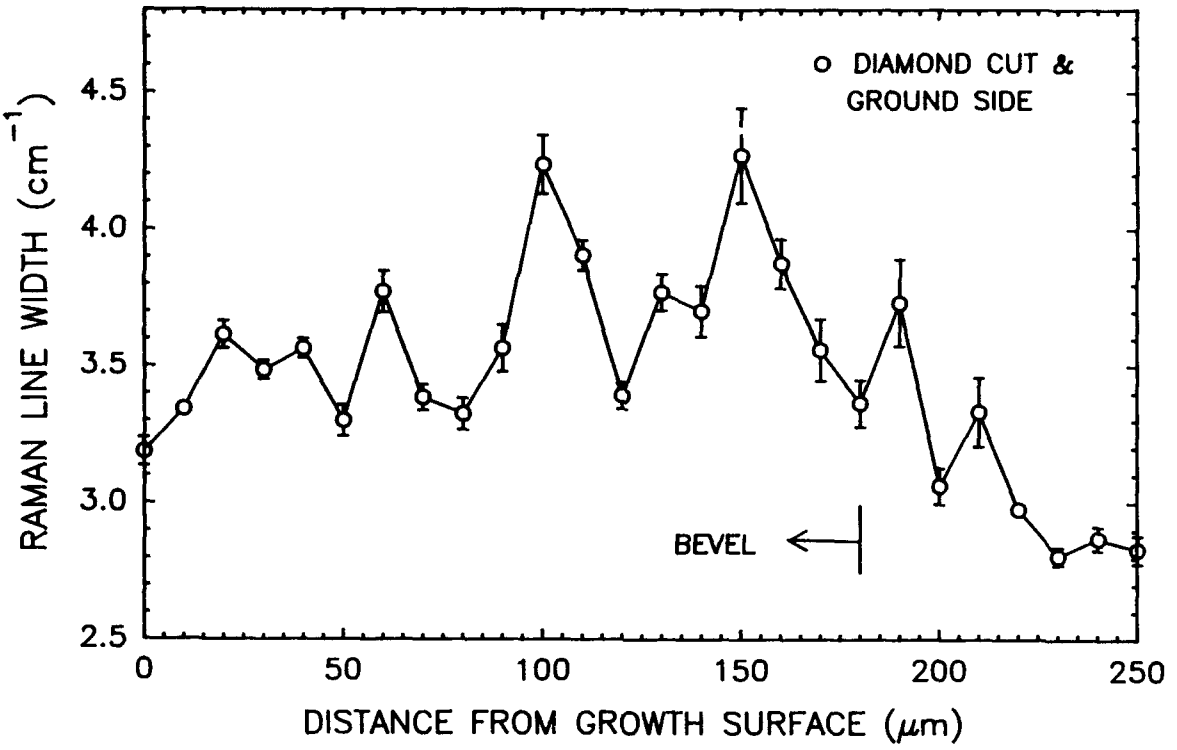

Figure 18. Raman scan on the diamond cut end 3500 μm from the growth surface of the specimen.

by the open circles. Fitting uncertainties in the widths (see FWMH on the graphs) were typically 1.5 to 2.0 percent. These uncertainties are plotted as error bars on the graphs.

In materials where the optical penetration depth is small, typically ≤ 1 mm, the width of a Raman line is a sensitive indicator of the relative amount of residual stress in the near surface region. This width depends on the long range order of the crystal or crystallites being probed. In general, cleaved, single crystal surfaces will show the smallest width.

Surface processing, such as grinding or polishing, introduce localized strains which reduce the long range ordering of the local crystalline environment. This loss of order broadens the Raman line. For example, polishing with a coarse grit will broaden the line more than polishing with a fine grit. Thus, the broader the line, the greater the relative residual stress.

Since the specimens studied here are polycrystalline, the residual stress can vary from grain-to-grain, particularly in ground surfaces. This is clearly seen in Figures 14 and 15. In contrast, the data in Figure 15 for the cut end (no grinding or polishing) shows a constant width over more than 4 mm suggesting a uniform but small or zero residual stress as might be

expected. The data confirm the high precision of our results. Moreover, the cut end data strongly supports the conclusion that the bulk material has very small or zero strain gradients which suggests no bulk strains or nearly so.

A CVD SiC polished specimen surface (~3Å rms roughness) and its ground beveled (i.e., chamfered) edge were also scanned. Figure 19 shows a comparison of the Raman line broadening along the mirror surface and down along the side (or edge) of the mirror. Note the high residual strain in the polished surface versus the ground bevel. The figure shows clear evidence of a strain gradient over a distance of 0.3-0.4 mm in the beveled edge region. From there the width on the polished face are nearly uniform and significantly smaller than for the cut end data in Figure 15. This is consistent with the fineness of the final polishing step necessary to fabricate the mirror surface. The small deviations of the width are outside the fitting uncertainties and therefore may indicate some small nonuniform surface strains in the polished face. The data on the side of the mirror specimen shows the typical variations expected for a ground surface, but with somewhat smaller peak-to-peak variations than shown in Figures 14 and 15.

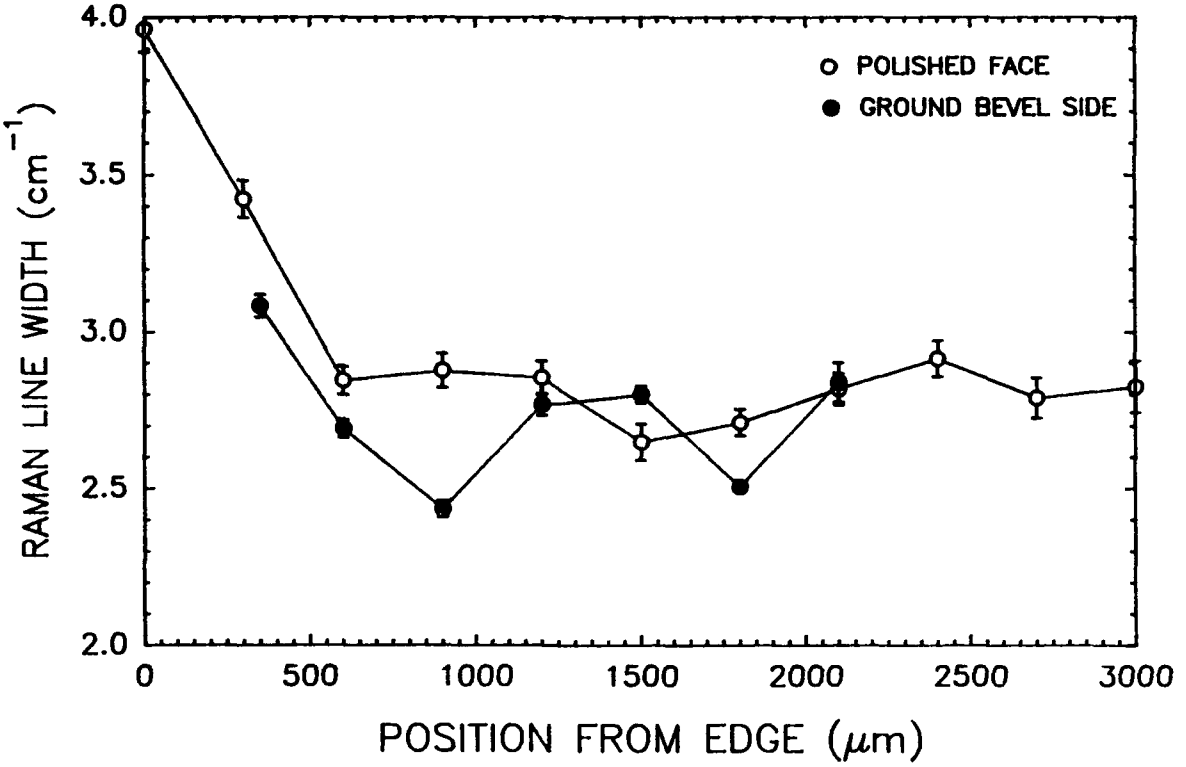

BEVEL IS ABOUT 310 μm WIDE. MEASUREMENTS ON THE MIRROR ARE ALONG A RADIUS FROM OUTER EDGE OF BEVEL. ON THE SIDE, THEY ARE ALONG A LINE PERPENDICULAR TO THE POLISHED FACE STARTING BELOW THE BEVEL.

Figure 19. Raman spectral line broadening due to residual strain on polished surface of the mirror specimen (surface roughness ~3Å rms) and the ground and beveled side (or edge).

CONCLUSIONS

From the test results obtained in this characterization study of CVD SiC, it can be concluded that:

- the material is chemically and crystallographically homogeneous;
- due to the long deposition run times required to deposit the material used in this study and resulting larger grain size, the average mechanical strength was slightly lower than the strength of material (~6 mm thick) from shorter deposition runs measured in previous studies;
- there is no statistically significant differences in mechanical strength when comparing material obtained from various locations within the bulk material;
- the thermal and optical properties were consistent for material taken from various locations within the bulk, further confirming the homogeneity of the material; and
- Raman microprobe spectroscopy indicated that there is no detectable residual strain gradients in the bulk SiC as deposited, however, detectable strain is present after grinding and polishing of the material.

ACKNOWLEDGMENTS

We thank Mr. William Kaveney and Mr. Donald Luczak of Rome Laboratory for their support in arranging for the funding to allow this program and their encouragement throughout the program. We thank Ms. Mary Dursi for aiding us in obtaining the subcontract to accomplish the work through her organization, Scientific Applications International Corporation.

We thank Mr. D. Wolf for the XRD work; Dr. P. Yaney for the Raman microprobe studies; Mr. S. Goodrich and Mr. D. McCullum for the mechanical property testing; Mr. D. Grant for the microstructural work; and especially Mr. S. Hilton for the preparation and arduous task of identifying and tracking the nearly two hundred specimens used in the study.

REFERENCES

1. Weibull, W., "A Statistical Distribution Function of Broad Applicability," J. Appl. Mech. 18(3), 1951, pp. 293-297.

2. Iden, D. J., Detrio, J. A., and Fox, J. A., "Optical Window Mechanical Strength and Reliability," AFWAL-TR-83-4059, June 1983, Contract F33615-80-C-5137.

3. Graves, G. A., McCullum, D. E., and Wimmer, J. M., "Investigation of the Thermal, Electrical, Mechanical, and Physical Properties of Infrared Laser Window and IR Transmitting Materials," AFML-TR-77-23, April 1977, Contract F33615-75-C-5011.

4. Lipson, C. and Sheth, N. J., Statistical Design and Analysis of Engineering Experiments, (McGraw Hill Book Co., NY, 1973).

5. Evans, A. G., "Fracture Mechanics Determinations," in Fracture Mechanics of Ceramics, Vol.2, ed. Bradt, R.C. (Plenum Press, NY, 1974).

6. Ritter, J. E., "Engineering Design and Fatigue Failure of Brittle Materials," in Fracture Mechanics of Ceramics, Vol. 4, ed. Bradt, R.C. (Plenum Press, NY, 1978).

7. Smyth, K. K. and Magida, M. B., "Dynamic Fatigue of a Machinable Glass Ceramic," J. Amer. Cer. Soc., 66(7), July 1983, pp. 500-505.

DISTRIBUTION LIST

addresses	number of copies
ROME LABORATORY/OCPC ATTN: RICHARD FEDORS 25 ELECTRONIC PKY GRIFFISS AFB NY 13441-4515	5
UNIVERSITY OF DAYTON RESEARCH INSTITUTE DAYTON, OH 45469-0172	5
RL/SUL TECHNICAL LIBRARY 26 ELECTRONIC PKY GRIFFISS AFB NY 13441-4514	1
ADMINISTRATOR DEFENSE TECHNICAL INFO CENTER DTIC-FDAC CAMERON STATION BUILDING 5 ALEXANDRIA VA 22304-6145	2
BALLISTIC MISSILE DEFENSE ORGANIZATION 7100 DEFENSE PENTAGON WASH DC 20301-7100	2
NAVAL WARFARE ASSESSMENT CENTER GIDEP OPERATIONS CENTER/CODE QA-50 ATTN: E RICHARDS CORONA CA 91718-5000	1
ASC/ENEMS WRIGHT-PATTERSON AFB OH 45433-6503	1
AFIT/LDEE 2950 P STREET WRIGHT-PATTERSON AFB OH 45433-6577	1

WRIGHT LABORATORY/MLPO 1
ATTN: D.L. DENISON
WRIGHT-PATTERSON AFB OH 45433-6533

WRIGHT LABORATORY/MTEL 1
WRIGHT-PATTERSON AFB OH 45433

AUL/LSE 1
BLDG 1405
MAXWELL AFB AL 36112-5564

COMMANDING OFFICER 1
NAVAL AVIONICS CENTER
LIBRARY D/765
INDIANAPOLIS IN 46219-2189

COMMANDING OFFICER 1
NCCOSC RDTE DIVISION
CODE 02748, TECH LIBRARY
53560 HULL STREET
SAN DIEGO CA 92152-5001

CMDR 1
NAVAL WEAPONS CENTER
TECHNICAL LIBRARY/C3431
CHINA LAKE CA 93555-6001

CDR, U.S. ARMY MISSILE COMMAND 2
REDSTONE SCIENTIFIC INFO CENTER
AMSMI-RD-CS-R/ILL DOCUMENTS
REDSTONE ARSENAL AL 35898-5241

ADVISORY GROUP ON ELECTRON DEVICES 2
ATTN: DOCUMENTS
2011 CRYSTAL DRIVE,SUITE 307
ARLINGTON VA 22202

LOS ALAMOS NATIONAL LABORATORY 1
REPORT LIBRARY
MS 5000
LOS ALAMOS NM 87544

COMMANDER/USAISC 1
ATTN: ASQP-DO-TL
BLDG 61801
FT HUACHUCA AZ 85613-5000

SOFTWARE ENGINEERING INST (SEI) 1
TECHNICAL LIBRARY
5000 FORBES AVE
PITTSBURGH PA 15213

NSA 1
E323/HC
SAB2 DOOR 22
FORT MEADE MD 21055-6000

NSA 1
ATTN: D. ALLEY
DIV X911
9800 SAVAGE ROAD
FT MEADE MD 20755-6000

DOD 1
R31
9800 SAVAGE ROAD
FT. MEADE MD 20755-6000

DIRNSA 1
R509
9800 SAVAGE ROAD
FT MEADE MD 20775

DEFENSE TECHNOLOGY SEC ADMIN (DTSA) 1
ATTN: STTD/PATRICK SULLIVAN
400 ARMY NAVY DRIVE
SUITE 300
ARLINGTON VA 22202

OC TECHNICAL LIBRARY 1
ROME LABORATORY/OC
26 ELECTRONIC PKY
GRIFFISS AFB NY 13441-4514

ROME LABORATORY/OC 1
26 ELECTRONIC PKY
GRIFFISS AFB NY 13441-4514

LITTON SYS INC/ITEK OPTICAL SYS DIV 2
ATTN: MARY R. LATHAM/SR. LIBRARIAN
FOR: MR TOM PITTS
10 MAGUIRE ROAD
LEXINGTON, MA 02173-3199

LOCKHEED CORP/TECHNICAL INFO CTR 1
ATTN: SUZANNA STANEK, TECH LIB
FOR: MUH-FA CHEN, (0/66-60, B586W)
D/90, DCS-L102, BLDG 106/BOX 3504
SUNNYVALE, CA 94088-3504

MARTIN MARIETTA CORP/AEROSPACE 1
ATTN: JACKIE O. BUNTING
DIR: TECHNOLOGY DEVELOPMENT
P.O BOX 179
DENVER, CO 80201

BMDO/TNS 1
ATTN: ERWIN MYRICK
7100 DEFENSE PENTAGON
WASHINGTON D.C. 20301-7100

TRW SPACE & DEFENSE 1
ATTN: JERRY F. SAO/MARIE MORAN
SENIOR TECHNICAL LIBRARIAN
ONE SPACE PARK
REDONDO BEACH, CA 90278

GRUMMAN AEROSPACE CORP. 1
ATTN: EDWARD LEE
M/S D-01-23
1111 STEWART AVENUE
BETHPAGE NY 11714-3541

TINSLEY LABORATORIES INC. 1
ATTN: ROBERT JOHNSON
V.P. MARKETING
3900 LAKESIDE DRIVE
RICHMOND, CA 94806

W. J. SCHAFER ASSOCIATES 3
ATTN: GAYLE FEOLE/SECURITY
FOR: RICHARD DYER
200 LIBERTY PLAZA
ROME, NY 13440

THE AEROSPACE CORP./LIB ACQ GROUP 1
ATTN: P W GREEN
FOR: DR VIRENDRA MAHAJAN M5643
P.O. BOX 92957
LOS ANGELES, CA 90009-2957

DR MICHAEL PICKERING 1
MORTON INTERNATIONAL/CVD INC
185 NEW BOSTON ST
WOBURN MA 01801-6203

DR GEORGE GRAVES 1
UNIVERSITY OF DAYTON RESEARCH
300 COLLEGE PARK KL-165
DAYTON OH 45469-0172

HUGHES AIRCRAFT CO 1
ATTN: D. WEBB
FOR: DR ROGER WITHERINGTON
P.O. BOX 902 E1/E110
EL SEGUNDO, CA 90245

EASTMAN KODAK CO/GOVERNMENT SYS 1
ATTN: BUDA ROBERT
FOR: MR DON GILDNER
PO BOX 24939
ROCHESTER NY 14624

BALL AEROSPACE SYSTEMS DIVISION 1
ATTN: MR PETER WALKER/SECURITY
FOR: MR E. A. ROYBAL
P.O. BOX 1062
BOULDER, CO 80306-1062

NATIONAL AERONAUTICS & SPACE ADMIN 1
OPTICAL SYSTEMS BRANCH
ATTN: MR ROBERT ROOD, MS:E823
MARSHALL SPACE FLIGHT CENTER, AL
35812

ROCKWELL INTERNATIONAL CORP/ 1
ATTN: MR DONALD J. CARLSON
P.O. BOX 3105
3370 MIRALOMA AVE
ANAHEIM CA 92803-3105

DONALD LUCZAK 1
ROME LABORATORY/OCPC
25 ELECTRONIC PKY
GRIFFISS AFB NY 13441-4515

DR GEORGE RAMSEYER 1
525 BROOKS RD
GRIFFISS AFB NY 13441-4505

DR YOLANDA KING 1
PL/XPP
ABERDEEN AVE SE
KIRTLAND AFB NM 87117-5776

COL LANNY LARSON 1
PL/LI
3550 ABERDEEN AVE SE
KIRTLAND AFB NM 87117-5776

LW BRANTLEY 1
NASA MSFC
PS 05
MARSHALL SPACE FLIGHT CTR AL 35812

GORDON AUGASON 1
NASA AMES RESEARCH CENTER
N-245-6
MOFFETT FIELD CA 94035-1000

JOEL SHADY 1
US ARMY SDC/CSSD-KA-RH
106 WYNN DRIVE
HUNTSVILL AL 35807

GEORGE SLOAN 1
US ARMY SDC/CSSD-SD-O
106 WYNN DRIVE
HUNTSVILLE AL 35807

CAPT WILLIAM CAMERON 1
WL/MLBC
2341 P ST STE 1
WRIGHT-PATTERSON AFB OH 45433-7750

DR RON KERANS 1
WL/MLLM
2230 TENTH ST STE 1
WRIGHT-PATTERSON AFB OH 45433-7750

JIM WELLS MS-160 1
TELEDYNE BROWN ENGINEERING
300 SPARKMAN DR NW
HUNTSVILLE AL 35807

DR HAROLD BENNETT 1
NAWC
CODE C023103
CHINA LAKE CA 93555

DR DONALD DECKER 1
NAWC
CODE C02316
CHINA LAKE CA 93555

KIM VU 1
SMC/MGSS
185 DISCOVERER BLVD STE 1315
LOS ANGELES AFB CA 90245-4695

LTC AYDELOTTE 1
SMC/MGSS
185 DISCOVERER BLVD STE 1315
LOS ANGELES AFB CA 90245-4695

DR CHIA SHIH LEE 1
SMC/MGSS
185 DISCOVERER BLVD STE 1315
LOS ANGELES AFB CA 90245-4695

LTC SOLT 1
SMC/MGSE
185 DISCOVERER BLVD
LOS ANGELES AFB CA 90245-4695

ERIC HANSEN 1
GEMINI 8-M TELESCOPES PROJECT
950 NORTH CHERRY AVE
TUCSON AZ 85726-6732

*U.S. GOVERNMENT PRINTING OFFICE: 1994-510-117-50032

MISSION

OF

ROME LABORATORY

Mission. The mission of Rome Laboratory is to advance the science and technologies of command, control, communications and intelligence and to transition them into systems to meet customer needs. To achieve this, Rome Lab:

a. Conducts vigorous research, development and test programs in all applicable technologies;

b. Transitions technology to current and future systems to improve operational capability, readiness, and supportability;

c. Provides a full range of technical support to Air Force Materiel Command product centers and other Air Force organizations;

d. Promotes transfer of technology to the private sector;

e. Maintains leading edge technological expertise in the areas of surveillance, communications, command and control, intelligence, reliability science, electro-magnetic technology, photonics, signal processing, and computational science.

The thrust areas of technical competence include: Surveillance, Communications, Command and Control, Intelligence, Signal Processing, Computer Science and Technology, Electromagnetic Technology, Photonics and Reliability Sciences.